*Q. J. R. Meteorol. Soc.* (2005), **131**, pp. 1863–1892 doi: 10.1256/qj.04.143

# Resistance and heat-transfer laws for stable and neutral planetary boundary layers: Old theory advanced and re-evaluated

By SERGEJ S. ZILITINKEVICH[1,2]† and IGOR N. ESAU[2]

[1]*Division of Atmospheric Sciences, Department of Physical Sciences, University of Helsinki, Finland*
[2]*Nansen Environmental and Remote Sensing Centre/Bjerknes Centre for Climate Research, Bergen, Norway*

(Received 24 September 2004; revised 14 February 2005)

SUMMARY

The planetary boundary layer (PBL) resistance and heat-transfer laws express the surface fluxes of momentum and heat through the PBL governing parameters. Since the late sixties, the dimensionless coefficients ($A$, $B$ and $C$) in these laws were considered as single-valued functions of internal stability parameters: $\mu = u_*/|f|L_s$ in the steady state PBLs, or $h/L_s$ in the evolving PBLs ($u_*$ is the friction velocity, $f$ is the Coriolis parameter, $L_s$ is the surface Monin–Obukhov length, and $h$ is the PBL depth). Numerous studies revealed very wide spread of data in empirical plots of $A$, $B$ and $C$ versus $\mu$ or $h/L_s$. It is not surprising that the above laws, although included in all modern textbooks on boundary-layer meteorology, are not practically used. In the present paper the resistance and heat-transfer laws are revised, accounting for the free-flow stability, baroclinicity and the rise of a capping inversion. The coefficients $A$, $B$ and $C$ become functions not only of $\mu$ or $h/L_s$, but also of the external stability parameter $\mu_N = N/|f|$ (where $N$ is the Brunt–Väisälä frequency in the free atmosphere above the PBL), the parameter of baroclinicity $\mu_\Gamma = \Gamma/N$ (or the free-flow Richardson number $\mathrm{Ri} = (N/\Gamma)^2 = \mu_\Gamma^{-2}$, where $\Gamma$ is the geostrophic wind shear), and the ratio of the actual and equilibrium PBL depths $h/h_E$. Moreover, the coefficient $C$ is redefined to account for the effect of a capping inversion. It follows that $A$, $B$ and $C$ can be considered as single-valued functions of $\mu$ only in the steady-state, barotropic, nocturnal (that is short-lived) PBL. On the other hand, the advanced laws cover a wide range of the PBL regimes. They are validated through large-eddy simulations of different types of PBLs: truly neutral, conventionally neutral, nocturnal and long-lived. This new development explains why prior formulations performed so poorly, and promotes advanced resistance and heat-transfer laws as practical tools for use in environmental modelling applications.

KEYWORDS: Baroclinic shear Free-flow stability Large-eddy simulation Non-local turbulence Non-steady regime

## 1. INTRODUCTION

The resistance laws for the barotropic planetary boundary layer (PBL) are presented in modern textbooks on boundary-layer meteorology (e.g. Garratt 1992) and comprehensively discussed in recent papers of Hess and Garratt (2002a,b) and Zilitinkevich and Esau (2002), so they do not require detailed introductory explanations. These laws express the absolute value of the surface stress $|\boldsymbol{\tau}|_{z=0} = u_*^2$ ($u_*$ is the friction velocity, and $z$ is the height) and the cross-isobaric angle $\alpha$ (the angle between the surface stress and the geostrophic wind) through the PBL governing parameters:

$$\frac{k}{C_g}\cos\alpha = \ln(C_g \mathrm{Ro}) - \widetilde{A}, \tag{1a}$$

$$\frac{k}{C_g}\sin\alpha = \mp\widetilde{B}, \tag{1b}$$

where $C_g$ and Ro are the geostrophic drag coefficient and the surface Rossby number:

$$C_g = \frac{u_*}{G}, \quad \mathrm{Ro} = \frac{G}{|f|z_{0u}}. \tag{2}$$

† Corresponding author: FMI, Vuorikatu 15 A, P.O. Box 503, 00101 Helsinki, Finland.
e-mail Sergej.Zilitinkevich@fmi.fi

Here, $k$ is the von Karman constant (conventional value: $k = 0.4$), $\widetilde{A}$ and $\widetilde{B}$ are dimensionless coefficients, $f$ is the Coriolis parameter, $z_{0u}$ is the surface roughness length for momentum, $G$ is the geostrophic wind speed: $G^2 = u_g^2 + v_g^2$, with components $u_g \equiv -(\rho f)^{-1}\partial p/\partial y = G\cos\alpha$ and $v_g \equiv (\rho f)^{-1}\partial p/\partial x = G\sin\alpha$ (depth-constant in the barotropic PBL), $\rho$ is the air density, and $p$ is the atmospheric pressure. On the right-hand side (r.h.s.) of Eq. (1b), minus is applied to the northern hemisphere and plus to the southern hemisphere.

The potential-temperature resistance law analogous to Eq. (1) reads:

$$\frac{k_T}{C_{TR}} = \ln(C_g \mathrm{Ro}) - \widetilde{C}, \tag{3a}$$

$$C_{TR} = \frac{\theta_*}{\Delta\theta_{PBL}}, \tag{3b}$$

where $k_T$ is the von Karman constant for the temperature, $T$, (conventional value: $k_T = 0.4$), $\widetilde{C}$ is the same type of dimensionless coefficient as $\widetilde{A}$ and $\widetilde{B}$, $C_{TR}$ is the thermal resistance coefficient, $\theta_* = -F_{\theta s}u_*^{-1}$ is the temperature-scale based on the near-surface turbulent flux of potential temperature $F_\theta|_{z=0} = F_{\theta s}$, $\Delta\theta_{PBL} = \theta_h - \theta_0$ is the bulk increment in potential temperature across the boundary layer, $\theta_h = \theta|_{z=h}$ is the potential temperature at the PBL upper boundary (considered as a given parameter), and $\theta_0$ is the aerodynamic potential surface temperature.

The latter is defined through the logarithmic extrapolation of $\theta(z)$ down to the level $z = z_{0u}$. Needless to say, $\theta_0$ differs from the actual surface temperature $\theta_s$ (often referred to as the radiometric temperature). The difference $\theta_0 - \theta_s$ ranges up to several K over rough surfaces. Traditionally, it is expressed as:

$$\frac{\theta_0 - \theta_s}{\theta_*} = \frac{1}{k_T}\ln\frac{z_{0u}}{z_{0T}}, \tag{4}$$

where $z_{0T}$ is the roughness length for temperature (e.g. Zilitinkevich *et al.* 2001). When $z_{0T}$ becomes very uncertain (over partially vegetated land and some other very complex land surfaces) alternative approaches should be applied (see Mahrt and Vickers 2002). In any case, introducing the aerodynamic surface temperature allows separate consideration of the thermal resistances of the two layers of essentially different nature:

- the PBL—in terms of $\Delta\theta_{PBL} = \theta_h - \theta_0$, Eqs. (3),
- the roughness layer—in terms of $\theta_0 - \theta_s$, Eq. (4), or using other schemes.

The present paper focuses on the PBL resistance laws.

Equations (3) in combination with Eqs. (1) provide the PBL heat-transfer law:

$$F_{\theta s} = -u_*\theta_* = -C_g C_{TR} G \Delta\theta_{PBL}. \tag{5}$$

Equations (1) for the neutral PBL (with $\widetilde{A}$ and $\widetilde{B}$ treated as universal constants: $\widetilde{A} = \widetilde{A}_0$ and $\widetilde{B} = \widetilde{B}_0$) were derived by Rossby and Montgomery (1935) from a turbulence closure model, and later by Kazanski and Monin (1961) from more general similarity-theory reasoning. An overview of further studies of the resistance law for the atmospheric neutral PBL is given by Hess and Garratt (2002a,b) and Hess (2004).

Zilitinkevich *et al.* (1967) and Zilitinkevich and Chalikov (1968) extended Eqs. (1) to the stratified PBLs affected by the non-zero buoyancy fluxes at the surface.

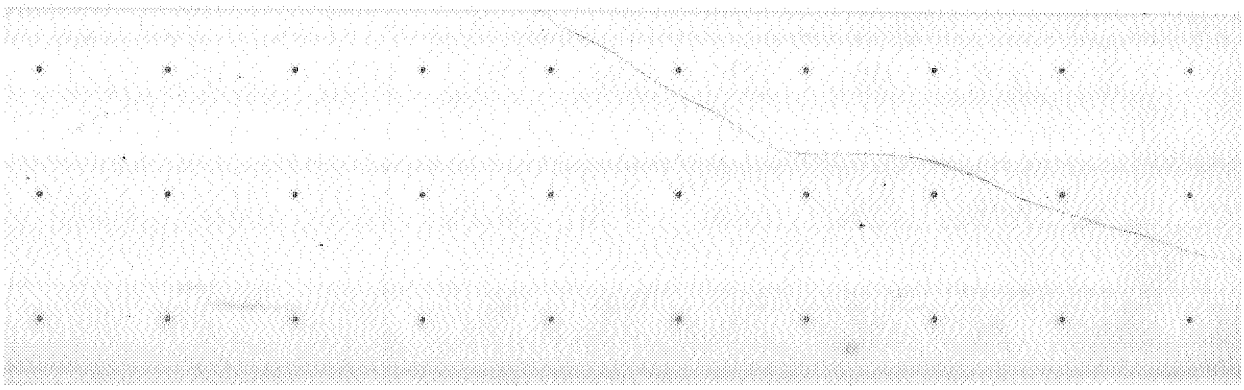

They showed that $\widetilde{A}$ and $\widetilde{B}$ depend on the internal stability parameter $\mu$ based on the Monin–Obukhov length scale $L_s$:

$$\mu = \frac{u_*}{|f|L_s}, \tag{6a}$$

$$L_s = \frac{-u_*^3}{\beta F_{\theta s}}, \tag{6b}$$

where $\beta = g/T$ is the buoyancy parameter, $g$ is the acceleration due to gravity, and $T$ is the absolute temperature. They also derived the temperature resistance law, Eqs. (3), with $\widetilde{C}$ dependent on $\mu$, and made the first attempt to empirically determine the resistance-law coefficients $\widetilde{A}$, $\widetilde{B}$, $\widetilde{C}$, and the similar type of coefficient $\widetilde{D}$ in the resistance law for humidity. In this context, the neutral stratification was defined as the regime in which $\mu$ is sufficiently small ($\mu < 10$). According to this point of view, the temperature flux $F_{\theta s}$ could be non-zero (and the heat-transfer law keeps its sense) when the stratification is practically neutral.

Zilitinkevich and Deardorff (1974) reformulated the resistance laws, employing the actual boundary-layer depth $h$ instead of the equilibrium PBL depth $h_E$ (or its basic scale $u_*/|f|$ employed in Eqs. (1)–(3)). The generalized laws read:

$$\frac{k}{C_g}\cos\alpha = \ln\frac{h}{z_{0u}} - A, \tag{7a}$$

$$\frac{k}{C_g}\sin\alpha = -\frac{fh}{u_*}B, \tag{7b}$$

$$\frac{k_T}{C_{TR}} = \ln\frac{h}{z_{0u}} - C. \tag{8}$$

Here, the resistance-law coefficients $A$, $B$ and $C$ are considered as functions of $h/L_s$ rather than $\mu$, which allows extension of the theory to non-steady boundary layers with time/space-dependent depths†. Equation (7b) is derived in section 2. In contrast to the prior formulation, $kC_g^{-1}\sin\alpha = \mp\widetilde{B}$, it explicitly shows that the cross-isobaric angle $\alpha$ is controlled by the Coriolis parameter $f$.

As for the stable stratification, all the above analyses were limited to the nocturnal PBLs, namely, the stable PBLs developed after sunset on the background of much deeper residual layers which were neutrally stratified due to intensive mixing during the daytime. In the steady-state nocturnal PBL (when the PBL depth $h$ is fully determined by $u_*$, $f$ and $L_s$, then $h = h_E = (u_*/|f|)f_h(\mu)$) Eqs. (7) and (8) reduce to Eqs. (1) to (3), wherein the coefficients $A$, $B$ and $C$ are expressed through $\widetilde{A}$, $\widetilde{B}$ and $\widetilde{C}$:

$$A = \widetilde{A} + \ln\frac{|f|h_E}{u_*}, \quad B = \pm\frac{u_*}{fh_E}\widetilde{B}, \quad C = \widetilde{C} + \ln\frac{|f|h_E}{u_*}. \tag{9}$$

Zilitinkevich (1975) determined asymptotic behaviours of the resistance-law coefficients in Eqs. (1) to (3) and (7) to (8) at large values of $\mu$ and $h/L_s$, respectively.

† Recall that convective PBLs never approach the steady state; they go on growing until the positive buoyancy flux is maintained. In contrast, stable PBLs tend to develop towards the steady state. The ratio $h/h_E$ is an important governing parameter for this type of turbulent boundary layer. Alternatively the deviation of the PBL from the steady state could be characterized by the dimensionless parameter $|f|h/u_*$ (Arya 1975).

In the steady-state truly neutral boundary layer, when the Monin–Obukhov length is large ($L_s \to \infty$, so that $\mu$, $h/L_s \to 0$) and the static stability in the airflow above the PBL is neutral, the equilibrium boundary-layer depth is expressed by the classical Rossby and Montgomery (1935) formula: $h_E = C_R u_*/|f|$, where $C_R$ is a dimensionless constant ($C_R = 0.7$, after laboratory experiments and LES†). Then the resistance law coefficients $\widetilde{A}_0$, $\widetilde{B}_0$, $\widetilde{C}_0$, where $A_0 = \widetilde{A}_0 + \ln C_R$, $B_0 = C_R^{-1}\widetilde{B}_0$ and $C_0 = \widetilde{C}_0 + \ln C_R$ become constants (subscript 0 indicates truly neutral stratification).

Since the late 1960s, particular cases of the above laws were independently derived (e.g. by Gill 1968), discussed and compared with experimental data in a large number of papers (see overviews in: Zilitinkevich 1989; Byun 1991; Hess and Garratt 2002a,b; Hess 2004). In the majority of these works, the PBL is considered to be neutral when $\mu$ or $h/L_s$ is zero or sufficiently small. In the 1970s and early 1980s, much work focused on experimental determination of the resistance-law coefficients $\widetilde{A}$, $\widetilde{B}$, $\widetilde{C}$ and $\widetilde{D}$, supposed to be single-valued functions of $\mu$. However, empirical relationships of this type showed such a wide spread of data that any interest in practical application of the resistance laws gradually decayed.

To some extent, large spreads of data on empirical plots of the coefficients $\widetilde{A}$ and $\widetilde{B}$ were explained at the expense of baroclinicity (e.g. Arya and Wynggard 1975; Joffre 1982, 1984). The baroclinic correction to the resistance law was formulated in a linear approximation, neglecting the effect of baroclinic shear on turbulent mixing. It included the following two steps. First, employing the surface values of the geostrophic wind components ($u_{g0} = u_g|_{z=0}$, $v_{g0} = v_g|_{z=0}$), the barotropic resistance law (with $\widetilde{A}$ and $\widetilde{B}$ dependent on $\mu$) was applied to determine $u_*$ and the 'barotropic part', $\alpha$, of the full wind-turn angle, $\alpha + \alpha_1$. Second, the 'baroclinic part' of this angle, $\alpha_1$, was determined as the full turn of the geostrophic wind across the PBL. A recent version of this model and an overview of prior work are given by Djolov *et al.* (2004).

It was recognized long ago that not only baroclinicity, but the depth and the strength of the capping inversions and the static stability in the free atmosphere affect bulk features of stable PBLs (e.g. Csanady 1974; Byun, 1991; Overland and Davidson 1992; King and Turner 1997). But the first attempts to quantify these effects were made only recently (Zilitinkevich *et al.* 1998; Zilitinkevich and Esau 2002, 2003).

A new theoretical model presented in this paper goes further, and extends the resistance and heat-transfer laws to long-lived, stable PBLs thereby accounting for the following mechanisms:

- Damping effect of the static stability in the free atmosphere on the PBL turbulent-length scale;
- Development of capping inversions at the PBL upper boundary;
- Enhancing effect of the baroclinic shear on the PBL turbulent-velocity scale.

Prior models overlooked these mechanisms and were therefore applicable only to the nocturnal PBLs. This explains the enormous spread of data points in old empirical plots of $\widetilde{A}$, $\widetilde{B}$, $\widetilde{C}$ and $\widetilde{D}$ versus $\mu$.

† Atmospheric data give much lower and very uncertain estimates of $C_R$ (e.g. Tjernstrom and Smedman 1993). This is due to the fact that the atmospheric boundary layers usually considered as neutral (according to the criteria $L_s \to \infty$ or $\mu \to 0$) are, in fact, only conventionally neutral; Zilitinkevich and Esau (2002) and Hess (2004) have demonstrated that their depths are strongly affected by the static stability in the free atmosphere.

TABLE 1. LARGE-EDDY SIMULATION ESTIMATES OF EMPIRICAL CONSTANTS

| Constant | Empirical value | Formula containing constant | Equation number |
|---|---|---|---|
| $C_b$ | 0.67 | $u_T = u_*^2(1 + C_b\mu_\Gamma)$ | (11) |
| $C_{NM}$<br>$C_{NH}$<br>$C_{fM}$<br>$C_{fH}$ | 0.1<br>1.5<br>1<br>1 | $\frac{1}{L_{\{M,H\}}} = \left\{\left(\frac{1}{L}\right)^2 + \left(\frac{C_{\{NM,NH\}}}{L_N}\right)^2 + \left(\frac{C_{\{fM,fH\}}}{L_f}\right)^2\right\}^{1/2}$ | (14) |
| $C_u$<br>$k$ | 2.5<br>0.47 | $\frac{\partial u}{\partial z} = \frac{\tau^{1/2}}{kz}\left(1 + \frac{C_u z}{L_M}\right)$ | (15) |
| $a$<br>$a_0$ | 1.4<br>1.65 | $A = -am_A + \ln(a_0 + m_A)$ | (41a) |
| $b$<br>$b_0$ | 10<br>−2 | $B = b_0 + bm_B^2$ | (41b) |
| $C_{NA}$<br>$C_{fA}$ | 0.09<br>1 | $m_A = \left\{\left(\frac{h}{L_s}\right)^2 + \left(\frac{C_{NA}h}{L_N}\right)^2 + \left(\frac{C_{fA}h}{L_f}\right)^2\right\}^{1/2}$ | (42) |
| $C_{NB}$<br>$C_{fB}$ | 0.15<br>1 | $m_B = \left\{\left(\frac{h}{L_s}\right)^2 + \left(\frac{C_{NB}h}{L_N}\right)^2 + \left(\frac{C_{fB}h}{L_f}\right)^2\right\}^{1/2}$ | (43) |
| $C_\theta$<br>$k_T$ | 2<br>0.47 | $\frac{\partial\theta}{\partial z} = \frac{\theta_*}{k_T z}\left(1 + \frac{C_\theta z}{L_H}\right)$ | (48) |
| $c$<br>$c_0$ | 4.1<br>12 | $C = -cm_C + \ln(e^{c_0} + m_C) \approx c_0 - cm_C$ | (56) |
| $C_{NC}$<br>$C_{fC}$ | 1.2<br>1 | $m_C = \left\{\left(\frac{h}{L_s}\right)^2 + \left(\frac{C_{NC}h}{L_N}\right)^2 + \left(\frac{C_{fC}h}{L_f}\right)^2\right\}^{1/2}$ | (57) |

In this paper, the free atmosphere is characterized by the Brunt–Väisälä frequency, $N$, and the baroclinic shears, $\Gamma_u = \partial u_g/\partial z$ and $\Gamma_v = \partial v_g/\partial z$, which involve the dimensionless parameters of the external stability $\mu_N$ and baroclinicity $\mu_\Gamma$:

$$\mu_N = \frac{N}{|f|}, \quad \text{where } N = \left(\beta\frac{\partial\theta}{\partial z}\right)^{1/2} \text{ at } z > h,$$

$$\mu_\Gamma = \frac{\Gamma}{N}, \quad \text{where } \Gamma = (\Gamma_u^2 + \Gamma_v^2)^{1/2} = \frac{g}{|f|T}\left\{\left(\frac{\partial T}{\partial y}\right)^2 + \left(\frac{\partial T}{\partial x}\right)^2\right\}^{1/2}. \tag{10}$$

Alternatively, the role of baroclinicity can be characterized by the free-flow Richardson number, $\mathrm{Ri} = \mu_\Gamma^{-2}$. On the r.h.s. of Eq. (10) for $\Gamma$, the geostrophic shear is expressed through the large-scale horizontal temperature gradient using the thermal-wind equation. $N$ and $\Gamma$ are taken to be depth-constant in a reasonable correspondence with observations in the earth's atmosphere: $N = 10^{-2}\ \mathrm{s}^{-1}$ and $\Gamma \sim (3-6)\cdot 10^{-3}\ \mathrm{s}^{-1}$, that correspond to $\mu_N \sim 10^2$ and $\mu_\Gamma \sim (3-6)\cdot 10^{-1}$.

Following Zilitinkevich and Esau (2003), the PBL baroclinic turbulent-velocity scale $u_T$ is defined as:

$$u_T^2 = \frac{u_*^2}{1 - C_b\mathrm{Ri}^{-1/2}} \approx u_*^2(1 + C_b\mathrm{Ri}^{-1/2}) = u_*^2(1 + C_b\mu_\Gamma), \tag{11}$$

where $C_b = 0.67$ is a dimensionless constant determined through LES validation of the baroclinic PBL depth formulation†. In the barotropic PBLs, $u_T$ reduces to the universally accepted scale $u_*$.

A list of estimates of empirical constants, such as $C_b$, obtained through LES is given in Table 1, together with the equations in this paper involving them.

Accounting for the $\mu_N$-dependence, Zilitinkevich and Esau (2002) have explained the wide spread of empirical data on $\widetilde{A}$ and $\widetilde{B}$, as well as a seemingly paradoxical disagreement between estimates in the atmosphere and estimates from LES, direct numerical simulation and laboratory experiments of $\widetilde{A}$ and $\widetilde{B}$ in boundary layers traditionally considered as neutral. The key point is that numerical or laboratory models deal with the truly neutral PBLs ($\mu = 0$ and $\mu_N = 0$), whereas atmospheric PBLs treated as neutral ($|\mu| \ll 10$) are nearly always strongly affected by the free-flow stability ($\mu_N \sim 10^2$). These two types of PBL are essentially different in nature. To distinguish between them, Zilitinkevich and Calanca (2000) have proposed the following definitions: the PBL is called 'conventionally neutral' when the buoyancy flux $\beta F_\theta$ approaches zero at the surface but the free flow above the PBL is stably stratified; the PBL is called 'truly neutral' when both the surface buoyancy flux, $\beta F_{\theta s}$, and the free-flow Brunt–Väisälä frequency, $N$, are zero.

In the present paper the theory is further advanced and validated against new LES.

## 2. THEORETICAL MODEL

### (a) *Turbulent-length scales*

Earlier versions of the resistance and heat-transfer laws were derived through asymptotic matching of the near-surface profiles of the wind velocity components $u(z)$, $v(z)$ and the potential temperature $\theta(z)$, with the defect-functions $u(z) - u(h)$, $v(z) - v(h)$ and $\theta(z) - \theta(h)$ in the overlapping height interval $z_{0u} \ll z \ll h$. Thus the surface-layer model represented an essential starting point of the theory.

Prior derivations employed the Monin–Obukhov (1954) similarity theory for the surface-layer profiles and the defect functions based on the PBL-depth formulations of Rossby and Montgomery (1935) and Zilitinkevich (1972) for the neutral and stable boundary layers, respectively.

This approach is justified when applied to nocturnal stable PBLs, i.e. to the comparatively short-lived PBLs separated from the free flow by a neutrally stratified residual layer, which keeps a 'memory' of the daytime mixing. In such PBLs, except for the thin logarithmic boundary layer close to the surface, the turbulent-length scale is limited to the 'local Monin–Obukhov length' $L$, defined similarly to Eq. (6b) but employing local ($z$-dependent) values of the turbulent fluxes of momentum, $\tau(z)$, and potential temperature, $F_\theta(z)$ (Nieuwstadt 1984).

More generally, including the truly neutral PBLs (in which $L^{-1} = 0$) and the long-lived stable PBLs (that is the PBLs bordering upon the stably stratified free atmosphere, without any intermediate residual layer), the turbulent-length scales are restricted by the following alternative limits: local ($z$-dependent) static-stability scale $L$, non-local external static-stability scale $L_N$, and the rotational scale $L_f$, namely:

$$L = \frac{\tau^{3/2}}{-\beta F_\theta}, \quad L_N = \frac{u_*}{N}, \quad L_f = \frac{u_*}{|f|}. \tag{12}$$

† In the imaginary case that the free atmosphere is neutrally stratified ($N = 0$) but baroclinic ($\Gamma > 0$), the baroclinic shear causes the overall generation of turbulence, so that the very concepts of the turbulent boundary layer and the PBL turbulent-velocity scale become inapplicable.

In baroclinic PBLs, the baroclinic turbulent-velocity scale $u_T$, Eq. (11), should be substituted for $u_*$ in the above expression for $L_N$.

The scales $L$ and $L_N$ are inherent to the nocturnal and to the conventionally neutral PBLs, and reflect the damping effect on turbulence of the turbulent buoyancy flux within the PBL and the static stability in the free flow, respectively. Clearly, in each concrete case the basic role is played by the stronger effect, that is by the smaller scale: $L$, $L_N$ or $L_f$. Moreover, their relative importance is different at different heights because $L$ depends on $z$ through the relationships $\tau(z)$ and $F_\theta(z)$.

In further analysis, we employ a recently created LES database representing three different types of stable PBL: nocturnal; long-lived and conventionally neutral; and the truly neutral PBL (see section 3). LES data shown in Fig. 1 demonstrate that the normalized fluxes of momentum and potential temperature can to a reasonable accuracy be considered as self-similar functions of the dimensionless height $\zeta = z/h$:

$$\frac{\tau}{u_*^2} = f_\tau(\zeta), \quad \frac{F_\theta}{F_{\theta s}} = f_{F\theta}(\zeta). \tag{13}$$

As shown in the appendix, such a self-similarity is consistent with scaling analysis of the Ekman equations. It has also been disclosed in prior analyses of field data (e.g. Lenshow *et al.* 1988; Sorbjan 1988; Wittich 1991). Within the PBL, the power-law approximations based on the field experiments over the Great Plains of the USA, $f_\tau(\zeta) = (1-\zeta)^{3/2}$ and $f_{F\theta}(\zeta) = 1-\zeta$, are quantitatively quite close to the exponential approximations: $f_\tau(\zeta) = \exp(-8/3\zeta^2)$ and $f_{F\theta}(\zeta) = \exp(-2\zeta^2)$, which better fit LES data in Fig. 1, and correspond to smooth decay of turbulence rather than its abrupt cut off at the PBL boundary.

It follows that the ratio $L/L_N$ and therefore the role of $L_N$ is small in the upper part of the PBL, and increases towards the surface. In other words, the role of the scale $L_N$ is most pronounced in the surface layer. This non-trivial conclusion is consistent with analyses of data from observations in presumably long-lived stable PBLs over Greenland (Zilitinkevich and Calanca 2000) and Antarctica (Sodemann and Foken 2004). New LES data shown in Fig. 2 (and, later, in Fig. 5) strongly support this conclusion.

It is worth emphasizing that our derivation of the resistance and heat-transfer laws is based on the assumption that the ratios $\tau/u_*^2$ and $F_\theta/F_{\theta s}$ are universal functions of $\zeta$, but concrete forms of these functions are not required.

Accounting for the alternative limits, $L$, $L_N$ and $L_f$, generalized turbulent-length scales, $L_{\{M,H\}}$, can be determined through the interpolation:

$$\frac{1}{L_{\{M,H\}}} = \left\{ \left(\frac{1}{L}\right)^2 + \left(\frac{C_{\{NM,NH\}}}{L_N}\right)^2 + \left(\frac{C_{\{fM,fH\}}}{L_f}\right)^2 \right\}^{1/2}, \tag{14}$$

which gives priority to the smaller scales. Dimensionless coefficients $C_{\{NM,NH\}}$ and $C_{\{fM,fH\}}$ can be different for the turbulent transports of momentum ($M$) and heat ($H$).

Recall that the scale $L_N$ was already applied to measure the PBL depth (Kitaigorodskii and Joffre 1988) and to generalize the Monin–Obukhov similarity theory for the surface layer (Zilitinkevich and Calanca 2000; Zilitinkevich 2002). The inverse quadratic interpolation between $L_s \equiv L|_{z=0}$ and $L_N$ was employed to derive an advanced PBL-depth model (Zilitinkevich and Baklanov 2002; Zilitinkevich and Esau 2002, 2003; Zilitinkevich *et al.* 2002).

Now, using the composite scale $L_M$ instead of $L$, and matching the log layer in the close vicinity of the surface and the $z$-less stratification layer aloft, the familiar velocity

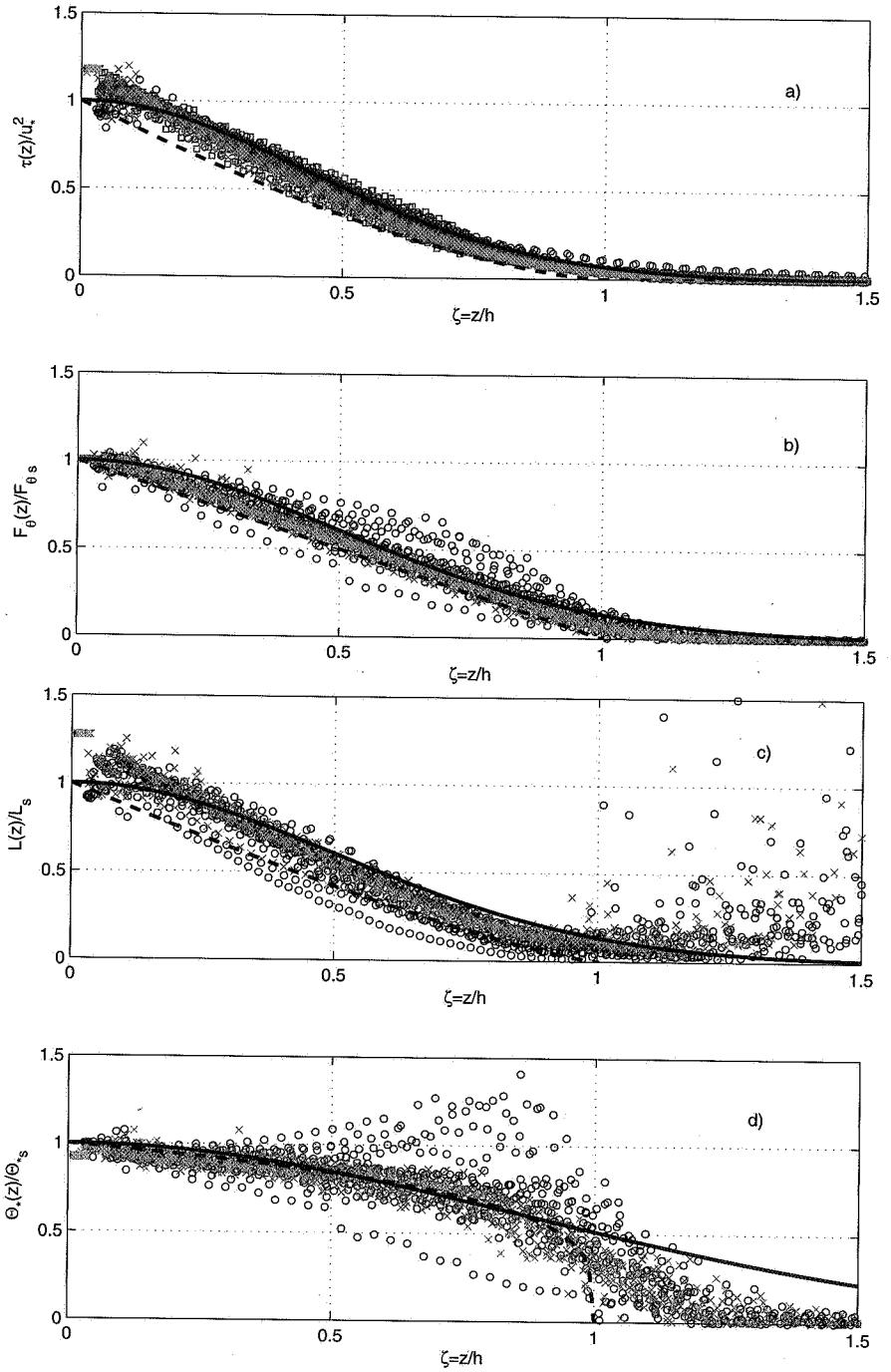


Figure 1. Normalized vertical profiles of: (a) turbulent flux of momentum $\tau/u_*^2$, (b) turbulent flux of potential temperature $F_\theta/F_{\theta s}$, (c) Monin–Obukhov length-scale $L/L_s$, and (d) potential-temperature-scale $\theta_*/\theta_{*s}$. The dimensionless height $\zeta = z/h$ is based on the planetary boundary layer (PBL) depth $h$. Large-eddy simulation (LES) data represent: nocturnal PBLs (crosses), long-lived PBLs (circles) and conventionally neutral PBLs (squares). Lines shown are: (a) $\tau/u_*^2 = \exp(-\frac{8}{3}\zeta^2)$ or $(1-\zeta)^{3/2}$; (b) $F_\theta/F_{\theta s} = \exp(-2\zeta^2)$ or $(1-\zeta)$; (c) $L/L_s = \exp(-2\zeta^2)$ or $(1-\zeta)^{5/4}$; (d) $\theta_*/\theta_{*s} = \exp(-\frac{2}{3}\zeta^2)$ or $(1-\zeta)^{1/4}$. Solid and dashed lines represent exponential- and power-law approximations, respectively. See text for further details.

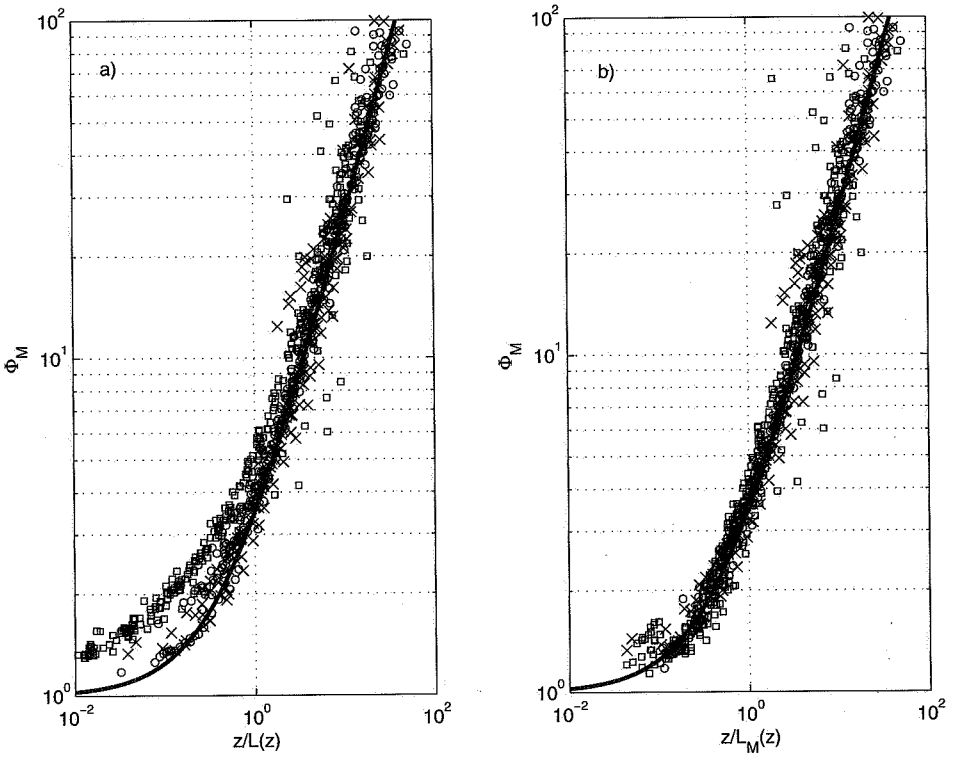


Figure 2. Dimensionless velocity gradient $\Phi_M = (kz/\tau^{1/2})(\partial u/\partial z)$ versus alternative dimensionless heights based on different $z$-dependent turbulent-length scales: (a) $z/L$, Eq. (12); (b) $z/L_M$, Eq. (14) with $C_{NM} = 0.1$, $C_{fM} = 1$. Large-eddy simulation (LES) data represent three different types of stable planetary boundary layers: nocturnal (crosses), long-lived (circles) and conventionally neutral (squares). The lines are: (a) traditional scaling $\Phi_M = 1 + 2.5z/L$; (b) multi-limit scaling $\Phi_M = 1 + 2.5z/L_M$. The best fit is achieved with $k = 0.47$. See text for further details.

gradient formulation becomes:

$$\frac{\partial u}{\partial z} = \frac{\tau^{1/2}}{kz}\left(1 + C_u\frac{z}{L_M}\right) \approx \frac{C_u\tau^{1/2}}{kL_M}, \tag{15}$$

where $C_u$ is a dimensionless constant. Recall that the '$z$-less stratification layer' is the height interval within the stably stratified turbulent flow in which the vertical size of turbulent eddies is controlled by negative buoyancy forces rather than the distance from the surface. Equation (15) differs from the Nieuwstadt (1984) formulation only due to the difference between $L_M$ and $L$.

Equation (15) affords an analytical expression of the eddy viscosity:

$$K_M = \frac{\tau}{\partial u/\partial z} = k\tau^{1/2}z\left(1 + C_u\frac{z}{L_M}\right)^{-1} \approx kC_u^{-1}\tau^{1/2}L_M. \tag{16}$$

Its approximate version, $K_M \approx kC_u^{-1}\tau^{1/2}L_M$, corresponds to the $z$-less stratification layer ($z \gg C_u^{-1}L$). Principally similar formulations for the potential-temperature gradient $\partial\theta/\partial z$, and the eddy conductivity $K_M$, are derived in subsection 2(d).

In the surface layer (at $z < 10^{-1}h$), substituting $u_*$ for $\tau^{1/2}$ and $F_{\theta s}$ for $F_\theta$ (then $L_M \to L_{Ms}$) and, neglecting the effects of the free flow stability and the earth's rotation

by taking $C_{NM}$, $C_{fM} = 0$ (then $L_{Ms} = L_s$), Eqs. (15) and (16) reduce to the traditional Monin–Obukhov similarity theory formulation. The latter has been verified against experimental data in numerous papers, which give estimates of $C_u$ in the interval $2 < C_u < 3$. As is evident from Eq. (14), this uncertainty can, at least partially, be caused by the difference between $L_s$ and $L_{Ms}$, and—in shallow PBLs—by unnoticed use of data beyond the surface layer. Indeed, factual length scales $L$ and $L_M$ decrease with increasing height (see Fig. 1), which inevitably leads to artificial overestimation of the coefficient $C_u$ if data analysis is based on the traditional depth-constant Monin–Obukhov length scale $L_s$.

Equation (15) is applied to the absolute value of the wind speed $|u| = (u^2 + v^2)^{1/2}$ rather that to its longitudinal component $u$ (aligned with the turbulent stress at the very surface). The contribution to $|u|$ from the transverse component $v$ caused by the Coriolis force is small in the surface layer but becomes significant above it.

Figure 2 shows the dimensionless velocity gradient $\Phi_M = (kz/\tau^{1/2})(\partial u/\partial z)$, as dependent on the two versions of the dimensionless height, $z/L$ in Fig. 2(a) and $z/L_M$ in Fig. 2(b), and include LES data from the entire PBL. It is seen that the generalized length scale $L_M$ (employed in Fig. 2(b)) provides uniform representation of the three different types of stable PBL (conventionally neutral, nocturnal and long-lived); by this means it leads to a better collapse of LES data than the traditional scale $L$. Moreover, this figure confirms applicability of Eq. (15) throughout the PBL and gives quite certain estimates of empirical constants: $k = 0.47$, $C_u = 2.5$, $C_{NM} = 0.1$ and $C_{fM} = 1$.

To derive a general form of the resistance law, we begin with the nocturnal PBL ($N = 0$ and $L_f \gg L$, so that $L_M = L$), we then consider the conventionally neutral PBL ($\beta F_{\theta s} = 0$ and $L_f \gg L$, so that $L_M = L_N$), and subsequently the truly neutral PBL ($N = 0$ and $\beta F_{\theta s} = 0$, so that $L_M = L_f$); finally we interpolate between the resistance laws inherent to these three types of the PBL.

### (b) *Resistance law for nocturnal PBLs*

In the surface layer ($z < 10^{-1}h$) within the barotropic nocturnal PBL ($\Gamma = 0$, $N = 0$, $L_f \gg L$), taking $\tau^{1/2} = u_*$ and $L = L_s$, Eq. (15) yields the following expressions for the longitudinal velocity component $u$:

$$\frac{\partial u}{\partial z} = \frac{u_*}{kz}\left(1 + C_u\frac{z}{L_s}\right) \approx \begin{cases} \dfrac{u_*}{kz} & \text{at } z \leqslant C_u^{-1}L_s \\ \dfrac{C_u u_*}{kL_s} & \text{at } z \geqslant C_u^{-1}L_s, \end{cases} \tag{17}$$

$$u \approx \begin{cases} \dfrac{u_*}{k}\ln\dfrac{z}{z_{0u}} & \text{at } z \leqslant C_u^{-1}L_s \\ \dfrac{u_*}{k}\left(\ln\dfrac{L_s}{C_u z_{0u}} + C_u\dfrac{z}{L_s} - 1\right) & \text{at } z \geqslant C_u^{-1}L_s. \end{cases} \tag{18}$$

Assuming that the vertical profiles of turbulent fluxes are self-similar, Eqs. (13) and (15) in the $z$-less stratification layer yield $\partial u/\partial z = k^{-1}C_u u_* L_s^{-1} f_u(\zeta)$, where $f_u(\zeta) = f_{F\theta} f_\tau^{-1}$. Then, to account for the effect of baroclinicity, we simply add the baroclinic wind shear $\Gamma_u$:

$$\frac{\partial u}{\partial z} = \frac{C_u u_*}{kL_s} f_u(\zeta) + \Gamma_u. \tag{19}$$

This additional term ensures the required upper-boundary condition $\partial u/\partial z \to \Gamma_u$, whereas in the surface layer the term $\Gamma_u$ is practically negligible compared to the main

term (see appendix of Zilitinkevich and Esau 2003). Integrating Eq. (19) over $z$ from an arbitrary height $z$ to the PBL upper boundary $z = h$ yields:

$$u(h) - u(z) = \frac{C_u u_* h}{k L_s} \Phi_u(\zeta) + \Gamma_u h (1 - \zeta). \tag{20}$$

Here, the function $\Phi_u$ is defined as $\Phi_u = \int_\zeta^1 f_u(\zeta)\, d\zeta$, and $u(h) = u_{gh}$ is the $u$-component of the geostrophic wind at the PBL upper boundary. The latter consists of the barotropic and baroclinic parts:

$$u(h) = u_{g0} + \Gamma_u h = G \cos\alpha + \Gamma_u h, \tag{21}$$

where $G$ and $\alpha$ are the surface values of the geostrophic wind speed and the cross-isobaric angle. Substituting Eq. (21) for $u(h)$ in Eq. (20) yields the longitudinal velocity defect function:

$$G \cos\alpha - u(z) = \frac{C_u u_* h}{k L_s} \Phi_u(\zeta) - \Gamma_u h \zeta, \tag{22}$$

which is valid in the height interval $L_s/h < \zeta < 1$.

Consider Eq. (22) in the $z$-less stratification part of the surface layer: $L_s/h < \zeta \ll 1$. Here, the term $\Gamma_u h \zeta$ is negligible because $\zeta \ll 1$. Then, substituting the lower line on the r.h.s. of Eq. (18) for $u(z)$ yields:

$$k \frac{G \cos\alpha}{u_*} - \ln \frac{L_s}{C_u z_{0u}} + 1 = C_u \frac{h}{L_s} \{\zeta + \Phi_u(\zeta)\} \equiv a \frac{h}{L_s} (a = \text{constant}). \tag{23}$$

The left-hand side (l.h.s.) of Eq. (23) does not depend on $\zeta$. Thus, in the overlapping region the combination $C_u\{\zeta + \Phi_u(\zeta)\}$ on the r.h.s. must be a dimensionless constant (assigned as $a$). Rearranging the terms in Eq. (23) yields the resistance law Eq. (7a) with the following $A$-coefficient:

$$A = -a \frac{h}{L_s} + \ln \frac{h}{L_s} + \ln C_u + 1 = -a \frac{h}{L_s} + \ln \frac{h}{L_s} + \text{constant}, \tag{24}$$

which holds true asymptotically at $h/L_s \gg 1$.

To determine the transverse velocity component, $v$, consider the Ekman equations:

$$f(v - v_g) + \frac{\partial \tau_x}{\partial z} = 0, \quad -f(u - u_g) + \frac{\partial \tau_y}{\partial z} = 0. \tag{25}$$

Here, $\tau_x$ and $\tau_y$ are the components of the vertical flux of momentum along the horizontal axes $x$ and $y$. The $x$-axis is aligned with the surface stress to make $\tau_y = 0$ at $z = 0$. Hence the boundary conditions are:

$$\begin{aligned} &u, v = 0, \quad \tau_x = u_*^2, \quad \tau_y = 0 \quad \text{at } z = 0; \\ &u \to u_g, \quad v \to v_g, \quad \tau_x, \tau_y \to 0 \quad \text{at } z \to \infty. \end{aligned} \tag{26}$$

Limiting our analysis to the $z$-less stratification part of the surface layer, we take $u(z)$ from the lower line on the r.h.s. of Eq. (18) and $u_g = G \cos\alpha$ from Eq. (23). This gives the longitudinal velocity-defect function:

$$u - u_g \approx \frac{C_u u_*}{k} \frac{h}{L_s} \left(\zeta - \frac{a}{C_u}\right). \tag{27}$$

Then, substituting Eq. (27) for $u - u_g$ in Eq. (25b), integrating over $z$ and accounting for the boundary condition $\tau_y|_{z=0} = 0$ gives the transverse component of

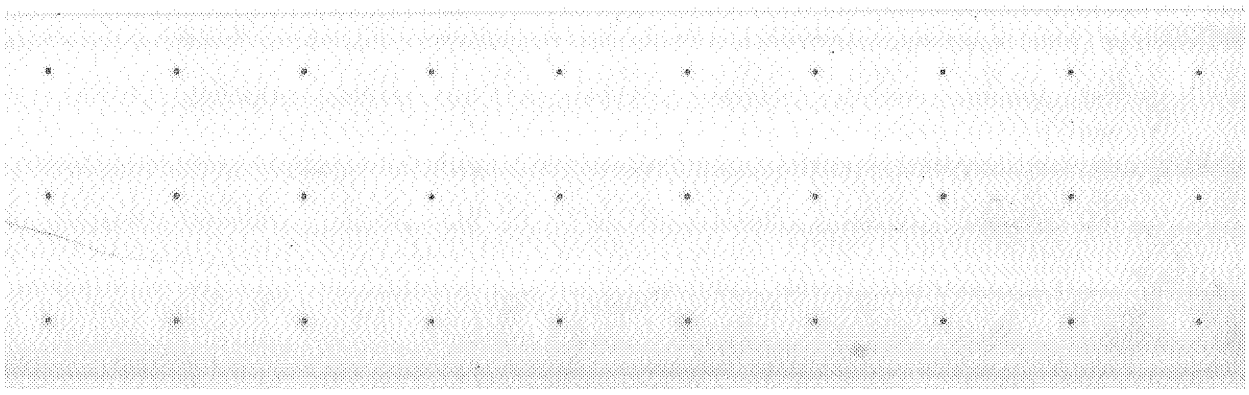

the momentum flux:

$$\tau_y = -\frac{afu_* h}{k}\frac{h}{L_s}\left(\zeta - \frac{C_u}{2a}\zeta^2\right) \approx -\frac{afu_* h}{k}\frac{h}{L_s}\zeta. \tag{28}$$

In the surface layer, the longitudinal component of this flux can be taken to be constant with depth: $\tau_x \approx \tau_x|_{z=0} = u_*^2$. Then Eq. (16) for the eddy viscosity reduces to:

$$K_M = ku_* z\left(1 + C_u\frac{z}{L_s}\right)^{-1}. \tag{29}$$

Next, $\partial v/\partial z$ and $v$ are determined:

$$\frac{\partial v}{\partial z} = \frac{\tau_y}{K_M} = -\frac{af}{k^2}\frac{h}{L_s}\left(1 + C_u\frac{z}{L_s}\right) \approx -\frac{C_u a}{k^2}\left(\frac{h}{L_s}\right)^2 f\zeta, \tag{30}$$

$$v \approx -\frac{C_u a}{2k^2}\left(\frac{h}{L_s}\right)^2 fh\zeta^2, \tag{31}$$

where approximate expressions correspond to the z-less stratification part of the surface layer.

To extend the surface-layer formulation, Eq. (30), to the upper portion of the PBL, we substitute $L(z) = L_s f_\tau^{3/2}(\zeta) f_{F\theta}^{-1}(\zeta)$ for $L_s$ and add the baroclinic wind shear, $\Gamma_v$, to the r.h.s. of the equation:

$$\frac{\partial v}{\partial z} = -\frac{C_u a}{k^2}\left(\frac{h}{L_s}\right)^2 f\zeta f_v(\zeta) + \Gamma_v, \tag{32}$$

where $f_v = f_{F\theta}^2 f_\tau^{-3}$ (recall the similar reasoning used in the derivation of Eq. (19)).

Integrating Eq. (32) over $z$ from $z$ to $h$ yields:

$$v(h) - v(z) = -\frac{C_u a}{k^2}\left(\frac{h}{L_s}\right)^2 fh\Phi_v(\zeta) + \Gamma_v h(1 - \zeta). \tag{33}$$

Here, $\Phi_v = \int_\zeta^1 f_v(\zeta)\zeta\, d\zeta$ is a universal function of $\zeta$, and $v(h) = v_{gh}$ is the $v$-component of the geostrophic wind at the PBL upper boundary, which consists of the barotropic and baroclinic parts:

$$v(h) = v_{g0} + \Gamma_v h = G\sin\alpha + \Gamma_v h. \tag{34}$$

Substituting Eq. (34) for $v(h)$ in Eq. (33) yields the transverse velocity-defect function:

$$G\sin\alpha - v(z) = -\frac{C_u a}{k^2}\left(\frac{h}{L_s}\right)^2 fh\Phi_v(\zeta) - \Gamma_v h\zeta, \tag{35}$$

valid in the height interval $L/h_s < \zeta < 1$. In the $z$-less stratification part of the surface layer, substituting Eq. (31) for $v(z)$ and neglecting the term $\Gamma_v h\zeta$, Eq. (35) reduces to:

$$k\frac{G\sin\alpha}{u_*} = -\frac{C_u a}{2k}\left(\frac{h}{L_s}\right)^2\frac{fh}{u_*}\{\zeta^2 + 2\Phi_v(\zeta)\} \equiv -b\frac{fh}{u_*}\left(\frac{h}{L_s}\right)^2 (b = \text{constant}). \tag{36}$$

Here, the combination $C_u a(2k)^{-1}\{\zeta^2 + 2\Phi_v(\zeta)\}$ turns into a universal dimensionless constant (assigned $b$) because the l.h.s. of Eqs. (36) does not depend on $\zeta$.

Equation (36) is nothing but the resistance law Eq. (7b) with the resistance-law coefficient:

$$B = b\left(\frac{h}{L_S}\right)^2. \tag{37}$$

Like Eq. (24), this expression holds true asymptotically at $h/L_S \gg 1$.

In the barotropic steady state, the nocturnal PBL depth becomes $h_E = C_S(L_S u_*/|f|)^{1/2}$, where $C_S \approx 1$ (e.g. Zilitinkevich and Esau 2003); so the dimensionless parameter in Eqs. (35)–(37) becomes $h/L_S = C_S\mu^{1/2}$, where $\mu$ is the traditional internal stability parameter, Eq. (6a). Recall that the very concept of the nocturnal PBL (that is the stable PBL with zero static stability in the free flow: $N = 0$) loses its sense in the baroclinic atmosphere. Indeed, in the case that $N = 0$ but $\Gamma > 0$ the shear-generated turbulence would appear throughout the troposphere.

### (c) *Extension of the theory to other types of PBLs*

The above analysis is immediately applicable to the conventionally neutral PBL, with the only principal difference being that the local Monin–Obukhov length scale $L(z)$, Eq. (12a), and its surface value $L_S = -u_*^3(\beta F_{\theta S})^{-1}$ are both substituted by the depth-constant length-scale $C_{NM}^{-1}L_N$, where $C_{NM}$ is a dimensionless constant (after Fig. 2, $C_{NM} = 0.1$). Thus in the conventionally neutral PBL the vertical gradients of the velocity components are expressed by formulae similar to Eqs. (19) and (32) but based on the length scale $L_N = u_*/N$:

$$\frac{\partial u}{\partial z} = \frac{C_u C_{NM} u_*}{kL_N} f_{uN}(\zeta) + \Gamma_u, \quad \frac{\partial v}{\partial z} = -\frac{C_u C_{NM}^2 a}{k^2}\left(\frac{h}{L_N}\right)^2 f\zeta f_{vN}(\zeta) + \Gamma_v, \tag{38}$$

with the correction functions $f_{uN}(\zeta)$ and $f_{vN}(\zeta)$ different from the functions $f_u(\zeta) = f_{F\theta}(\zeta)f_\tau^{-1}(\zeta)$ and $f_v(\zeta) = f_{F\theta}^2(\zeta)f_\tau^{-3}(\zeta)$ that appeared in Eqs. (19) and (32). It follows that the resistance-law Eqs. (7) hold true, but the coefficients $A$ and $B$ become functions of $h/L_N$:

$$A = -a_N\frac{C_{NM}h}{L_N} + \ln\frac{C_{NM}h}{L_N} + \text{constant}, \quad B = b_N\left(\frac{C_{NM}h}{L_N}\right)^2, \tag{39}$$

where $a_N$ and $b_N$ are dimensionless empirical constants different from $a$ and $b$, $C_{NM} = 0.1$ is the constant already determined from Fig. 2. Equations (39) are asymptotic expressions corresponding to $C_{NM}h/L_N \gg 1$.

In the barotropic steady state, the conventionally neutral PBL depth becomes $h_E = C_C u_*(|f|N)^{1/2}$, where $C_C \approx 1.3$ (see Zilitinkevich and Esau 2003); so that the dimensionless parameter in Eq. (39) becomes $h/L_N = C_C\mu_N^{1/2}$, where $\mu_N$ is the external stability parameter, Eq. (10a). This result also holds true in the baroclinic regime, when $h_E = C_C u_T(|f|N)^{1/2}$ and $L_N = u_T/N$. Thus the effect of baroclinicity on the resistance-law coefficients manifests itself only through the dependence of $h$ on the parameter of baroclinicity $\mu_\Gamma$, Eq. (10b).

Similarly to the above analysis, in the truly neutral PBLs the turbulent-length scale is $L_f = u_*/|f|$. Then $A$ and $B$ become functions of $h/L_f$:

$$A = -a_f\frac{C_{fM}h}{L_f} + \ln\frac{C_{fM}h}{L_f} + \text{constant}, \quad \text{and } B = b_f\left(\frac{C_{fM}h}{L_f}\right)^2, \tag{40}$$

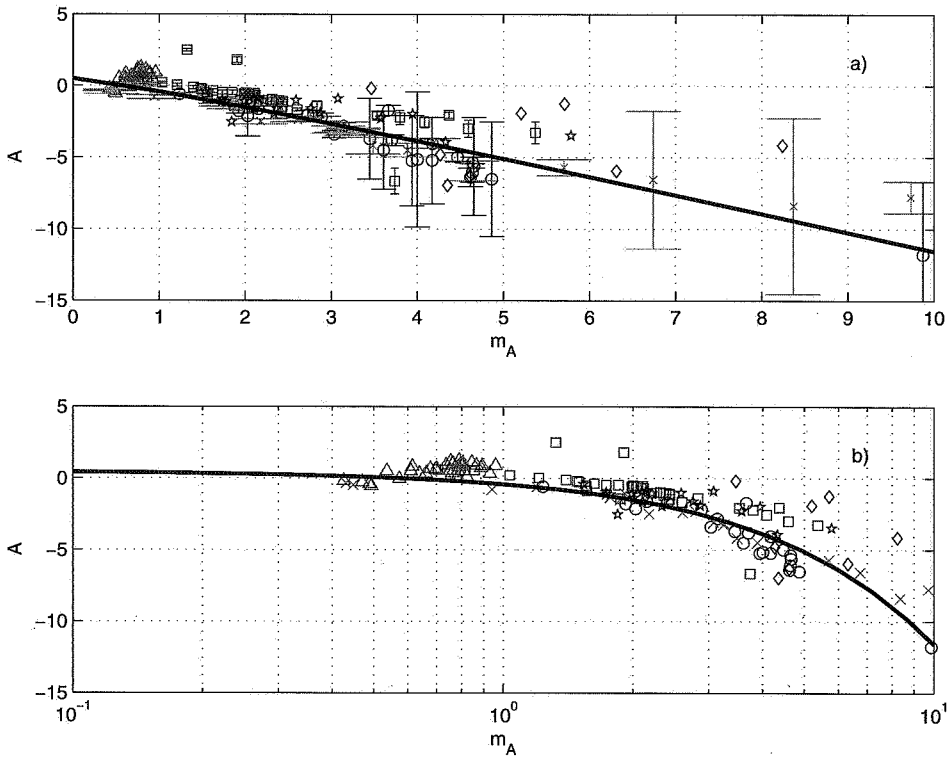


Figure 3. Large-eddy simulation (LES) data on the geostrophic-drag resistance-law coefficient $A = \ln(h/z_{0u}) - k(u_g/u_*)$ (with $k = 0.47$) versus the composite stratification parameter $m_A$, Eq. (42), with $C_{NA} = 0.09$, $C_{fA} = 1$. Data points represent new LES for: nocturnal PBLs (crosses), long-lived PBLs (circles) and conventionally neutral PBLs (squares). Earlier LES data, namely, Brown *et al.* 1994 (diamonds) and Kosovic and Curry 2000 (stars) do not show systematic deviations from new LES. Larger spread in old data of Brown *et al.* (1994) is to be expected because of the inevitably lower quality of the LES of that time. In (a) error bars show the ±3 standard deviation intervals for each LES run (with 96% statistical confidence); (b) employs log-linear coordinates to demonstrate how the theory performs in near-neutral and moderate-stability regimes. The line is $A = -1.4m_A + \ln(1.65 + m_A)$. See text for further details.

which each include an empirical constant $C_{fM} = 1$ (already determined from Fig. 2) and new constants $a_f$ and $b_f$. Generally, $h/L_f$ is a variable parameter; it tends to a constant ($h/L_f = C_R = 0.7$) only in the steady state when $h = h_E = C_R u_*/|f|$. As already mentioned, the above formula is very well confirmed by LES and laboratory experiment data, which give $C_R = 0.7$. The effect of baroclinicity is not relevant to this regime because the baroclinic shear ($\Gamma > 0$) on the background of the neutral static stability ($N = 0$) would inevitably result in the appearance of developed turbulence throughout the troposphere.

To link the three alternative resistance-law formulations, namely, Eqs. (24) and (37) for the nocturnal PBL, Eqs. (39) for the conventionally neutral PBL, and Eqs. (40) for the truly neutral PBLs, we employ the same inverse quadratic interpolation between the turbulent-length scales as in Eq. (14). This yields general expressions:

$$A = -am_A + \ln(a_0 + m_A), \tag{41a}$$

$$B = b_0 + bm_B^2, \tag{41b}$$

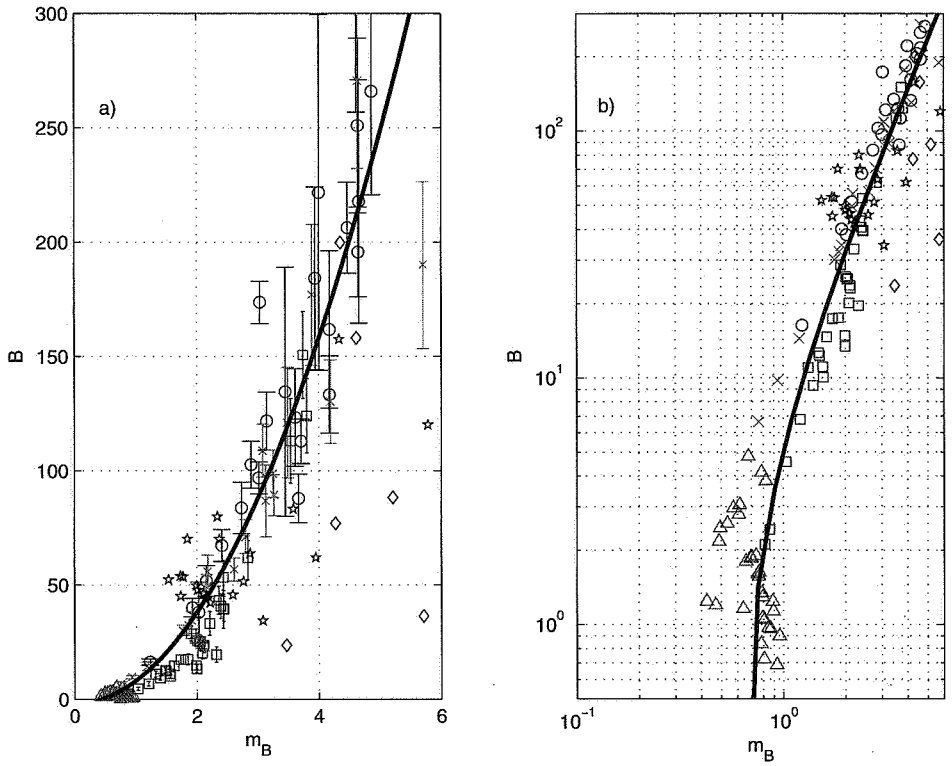


Figure 4. Same as in Fig. 3, but for the cross-isobaric-angle resistance-law coefficient $B = k(v_g/fh)$ (with $k = 0.47$) versus $m_B$, Eq. (43) with $C_{NB} = 0.15$, $C_{fB} = 1$. The lines show the theoretical dependence $B = -2 + 10m_B^2$. Notice that data points (shown as diamonds) are taken from older LES, which causes their larger spread. See text for further details.

where $m_A$ and $m_B$ are composite stratification parameters:

$$m_A = \left\{ \left(\frac{h}{L_s}\right)^2 + \left(\frac{C_{NA}h}{L_N}\right)^2 + \left(\frac{C_{fA}h}{L_f}\right)^2 \right\}^{1/2}, \tag{42}$$

$$m_B = \left\{ \left(\frac{h}{L_s}\right)^2 + \left(\frac{C_{NB}h}{L_N}\right)^2 + \left(\frac{C_{fB}h}{L_f}\right)^2 \right\}^{1/2}, \tag{43}$$

where $C_{NA} = C_{NM}a_N a^{-1}$, $C_{NB} = C_{NM}b_N b^{-1}$, $C_{fA} = C_{fM}a_f a^{-1}$, $C_{fB} = C_{fM}b_f b^{-1}$, $a_0$ and $b_0$ are dimensionless constants to be determined empirically.

LES data shown in Figs. 3 and 4 confirm Eqs. (41) to (43) and give quite certain estimates of the constants: $a = 1.4$, $a_0 = 1.65$, $C_{NA} = 0.09$, $C_{fA} = 1$; $b = 10$, $b_0 = -2$, $C_{NB} = 0.15$, $C_{fB} = 1$.

In the truly neutral PBLs $m_A \sim m_B \sim h/L_f$; hence $A$ and $B$ are functions of $h/L_f$. This explains the wide spread of data in prior estimates of the resistance-law coefficients for the truly neutral stratification. Only in the steady state (when $h \to h_E = C_R u_*/|f|$, so that $m_A$ and $m_B$ tend to non-zero limits: $m_A \to C_{fA}C_R = 0.7$ and $m_B \to C_{fB}C_R = 0.7$) do these coefficients turn into constants:

$$A \to A_0 = -aC_{fA}C_R + \ln(a_0 + C_{fA}C_R) = 0.07, \quad B \to B_0 = b_0 + bC_{fB}^2 C_R^2 = 2.9. \tag{44}$$

Notice that our stratification parameters $m_A$ and $m_B$ could be less than $C_{\{fA,fB\}}C_R = 0.7$ in the evolving neutral PBLs whose depths, $h$, do not approach the equilibrium limit, $h = h_E = C_R u_*/|f|$.

Equations (7) and (41) to (43) comprise the resistance law covering a range of neutral and stable PBL regimes, including long-lived stable PBLs and baroclinic PBLs. Recall that the traditional approach did not distinguish between the truly neutral and the conventionally neutral PBLs. Accordingly, in the traditional format (with $m_A = h/L_s$) all data representing different conventionally neutral PBLs would correspond to $h/L_s = 0$, thus causing a considerable spread of data points (cf. Figs. 10 and 11 in section 4).

In this context, $h$ is considered as a given parameter. In the steady state it is equal to the equilibrium stable PBL depth, $h_E$, controlled by the three dimensionless parameters: $\mu$, $\mu_N$ and $\mu_\Gamma$ (Zilitinkevich and Esau 2003). Thus our formulation accounts for the effect of baroclinicity on the resistance-law coefficients $A$ and $B$ through the dependence of $h_E$ on $\mu_\Gamma$, Eq. (10). In non-steady regimes, $h$ can be calculated using prognostic relaxation-type equation: $dh/dt \sim t_*^{-1}(h_E - h)$, where $t_* \sim h/u_*$ is the PBL relaxation time-scale (see subsection 3.2 in Zilitinkevich and Baklanov 2002).

### (*d*) *Proper PBL and capping inversion*

Notice that stable PBLs experience persistent cooling due to the negative (downward) heat flux at the surface $F_{\theta s} = F_\theta|_{z=0} < 0$. This cooling results in rising of the capping temperature inversion at the PBL upper boundary. Hence the temperature profile inevitably changes its shape in the course of time and the steady state is never achieved. At the same time, numerous experimental studies convincingly demonstrate that the temperature profile in the surface layer (at $z < 0.1h$) is at least approximately self-similar.

It looks reasonable to assume that the non-stationary changes are basically related to the capping inversion, whereas the temperature profile in the proper PBL shifts in a quasi-stationary manner, keeping its self-similar shape. This approach allows separate consideration of the two essentially different mechanisms:

- Maintaining a self-similar temperature profile in the proper PBL, controlled by instantaneous values of the turbulent fluxes of temperature and momentum and the free-flow Brunt–Väisälä frequency.
- Rising of the capping inversion and strengthening of the temperature increment $\Delta\theta_{CI}$ across it.

In the present paper we focus on the heat-transfer law for the proper PBL. Recall that the potential temperature in the free atmosphere (outside the PBL) is specified as a linear function of height: $\theta = \theta_{00} + \beta^{-1}N^2 z$. Then, given the PBL depth $h$, the basic-state potential temperature at the PBL upper boundary is an easily determined external parameter†:

$$\theta_{h+0} \equiv \theta_{00} + \frac{N^2}{\beta}h, \tag{45}$$

To distinguish between the proper PBL and the capping inversion, we determine the inversion half-depth, $\frac{1}{2}\delta_{CI}$, as the height interval between the PBL upper boundary, $z = h$, and the inflexion point just below this level, that is the height $z = h - \frac{1}{2}\delta_{CI}$, at which $\partial\theta/\partial z$ approaches a minimum ($\partial^2\theta/\partial z^2 = 0$) and starts increasing (then no inflexion point means no capping inversion). Considering the potential

† In our LES, $\theta_{00}$ is simply the initial value of $\theta$ at the surface: $\theta_{00} = \theta|_{z=0,t=0}$.

temperature at this height, $\theta_{h-0} \equiv \theta|_{z=h-\frac{1}{2}\delta_{CI}}$, as a reference value of $\theta$ at the upper boundary of the proper PBL, the potential-temperature increment across the capping inversion, $\Delta\theta_{CI}$, is defined as:

$$\Delta\theta_{CI} = \theta_{h+0} - \theta_{h-0}. \tag{46}$$

As already mentioned, we leave the theoretical determination of $\Delta\theta_{CI}$ for a separate paper, and limit our analysis to the derivation of the heat-transfer law for the proper PBL in terms of the potential-temperature increment across the PBL:

$$\Delta\theta_{PBL} = \theta_{h-0} - \theta_0. \tag{47}$$

Clearly, in the PBLs with no capping inversions (e.g. nocturnal PBLs) this definition reduces to the traditional one: $\Delta\theta_{PBL} = \theta_h - \theta_0 = \theta_{h+0} - \theta_0$.

Consider the similarity-theory formulation for the potential-temperature gradient:

$$\frac{\partial\theta}{\partial z} = \frac{\theta_*}{k_T z}\left(1 + \frac{C_\theta z}{L_H}\right), \tag{48}$$

based on the traditional turbulent temperature scale $\theta_* = -F_\theta \tau^{-1/2}$ and the generalized $z$-dependent turbulent-length scale $L_H$, Eq. (14). Equation (48) is derived similarly to Eq. (15), through matching the temperature-gradient scales $\theta_*/z$ and $\theta_*/L_H$ for the log-layer and the $z$-less stratification layer, respectively.

Figure 5 shows LES data on $\Phi_H = (k_T z/\theta_*)(\partial\theta/\partial z)$ as dependent on either $z/L$ (Fig. 5(a)) or $z/L_H$ (Fig. 5(b)) in the height interval $0 < z < h - \frac{1}{2}\delta_{CI}$ for the nocturnal (crosses) and long-lived (circles) stable PBLs†. It confirms applicability of Eq. (48) throughout the proper PBL, and demonstrates that our generalized scaling provides reasonably good collapse of practically all LES data taking the following values of dimensionless constants: $k_T = 0.47$, $C_\theta = 2$ and $C_{NH} = 1.5$. In other words, the scale $L_H$ is applicable to both nocturnal and long-lived PBLs in contrast to the traditional scale $L$ which applies only to the nocturnal PBLs.

Recalling the turbulent-flux profile approximations (given in Fig. 1), Fig. 5 supports an analytical eddy conductivity formulation‡:

$$K_H = \frac{-F_\theta}{\partial\theta/\partial z} = k_T \tau^{1/2} z\left(1 + C_\theta \frac{z}{L_H}\right)^{-1} \approx k_T C_\theta^{-1} \tau^{1/2} L_H, \tag{49}$$

where the approximate expression corresponds to the $z$-less stratification layer ($z \gg C_\theta^{-1} L$).

In further analysis we exclude the capping inversion layer and derive the heat-transfer law for the proper PBL.

† In the conventionally neutral PBLs the potential-temperature flux approaches zero at the surface: $F_\theta|_{z=0} = 0$. Hence, the temperature scale $\theta_*$ is inappropriate and data representing these PBLs cannot be shown in Fig. 5.

‡ Similar scaling reasoning in combination with analysis of LES data could be applied to derive a simple analytical formulation for the eddy diffusivity. Such a formulation could be useful in modelling the dispersion of pollution, especially in strong static-stability regimes, when traditional formulations often give poor results.

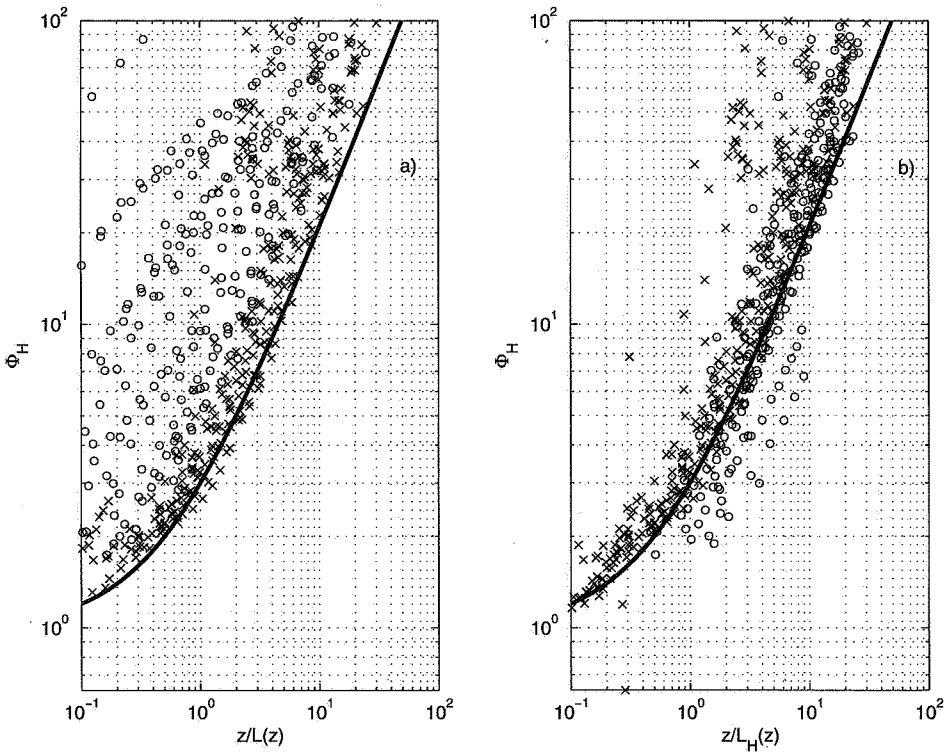


Figure 5. Dimensionless potential-temperature gradient $\Phi_H = (k_T \tau^{1/2} z/-F_\theta)(\partial\theta/\partial z)$ versus alternative dimensionless heights: (a) $z/L$ and (b) $z/L_H$ with $C_{NH} = 1.5$ and $C_{fH} = 1$. Crosses and circles represent nocturnal and long-lived planetary boundary layers (PBLs), respectively. Data on conventionally neutral PBLs are not included. The lines are: (a) $\Phi_H = 1 + 2z/L$; (b) $\Phi_H = 1 + 2z/L_H$. The best fit is achieved with $k_T = 0.47$. See text for further details.

### (e) *Heat-transfer law*

Consider first the nocturnal PBL. In the surface layer within this PBL, Eq. (48) yields:

$$\frac{\partial\theta}{\partial z} = \frac{\theta_{*s}}{k_T z}\left(1 + C_\theta \frac{z}{L_s}\right) \approx \begin{cases} \dfrac{\theta_{*s}}{k_T z} \text{ at } z \leqslant C_\theta^{-1} L_s \\ \dfrac{C_\theta \theta_{*s}}{k_T L_s} \text{ at } z \geqslant C_\theta^{-1} L_s, \end{cases} \tag{50}$$

$$\theta - \theta_0 \approx \begin{cases} \dfrac{\theta_{*s}}{k_T} \ln \dfrac{z}{z_{0u}} & \text{at } z \leqslant C_\theta^{-1} L_s \\ \dfrac{\theta_{*s}}{k_T}\left(\ln \dfrac{L_s}{C_\theta z_{0u}} + C_\theta \dfrac{z}{L_s} - 1\right) & \text{at } z \geqslant C_\theta^{-1} L_s. \end{cases} \tag{51}$$

In the $z$-less stratification part of the PBL (at $L(z) \ll z < h$), accounting for the self-similarity of the normalized turbulent fluxes, $\tau/u_*^2 = f_\tau(\zeta)$ and $F_\theta/F_{\theta s} = f_{F\theta}(\zeta)$, Eq. (48) reduces to:

$$\frac{\partial\theta}{\partial z} = \frac{C_\theta \theta_{*s}}{k_T L_s} f_\theta(\zeta), \tag{52}$$

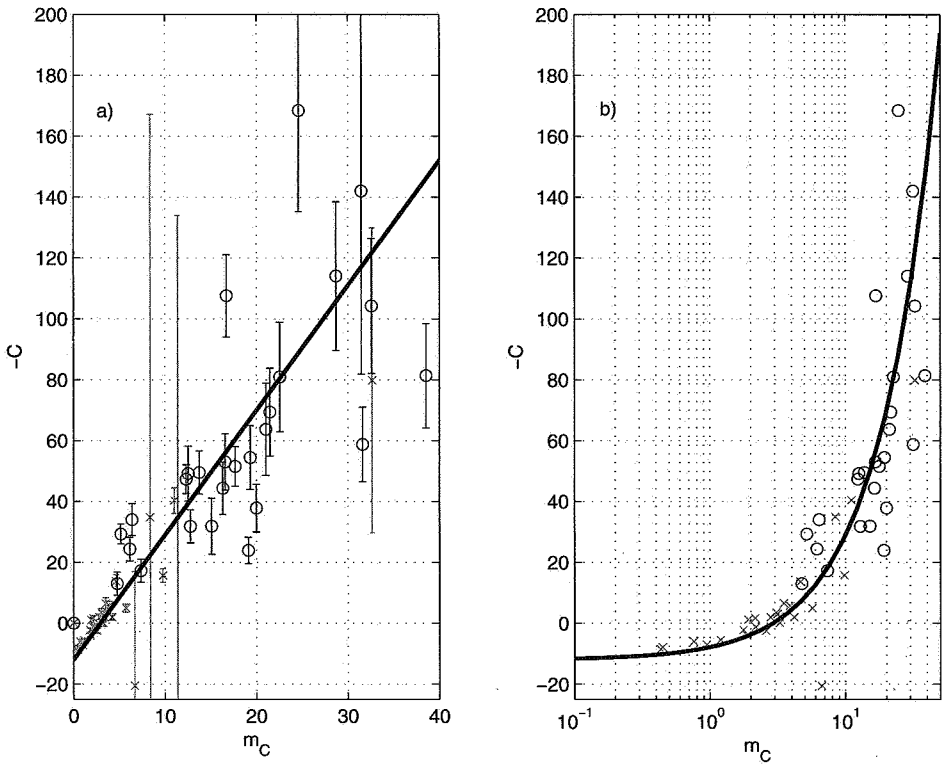


Figure 6. Same as in Figs. 3 and 4, but for the potential-temperature resistance-law coefficient $C = \ln(h/z_{0u}) - k_T(\Delta\theta_{\rm PBL}/\theta_{*\rm s})$ (with $k_T = 0.47$) versus $m_C$, Eq. (57) with $C_{NC} = 1.2$ and $C_{fC} = 1$. Data points represent new LES for nocturnal (crosses) and long-lived PBLs (circles); LES data for conventionally neutral PBLs are not included (here $\theta_{*\rm s} \to 0$, which is why the temperature resistance law loses physical meaning). The line is $C = -4.1m_C + \ln(e^{12} + m_C) \approx 12 - 4.1m_C$. See text for further details.

where $f_\theta = f_{F\theta}^2 f_\tau^2 \to 1$ at $\zeta \to 0$. Integrating Eq. (52) from $z$ to $h - \frac{1}{2}\delta_{\rm CI}$ yields the potential-temperature defect function:

$$\theta_{h-0} - \theta(z) = \frac{C_\theta(h - \frac{1}{2}\delta_{\rm CI})\theta_{*\rm s}}{k_T L_{\rm s}}\Phi_\theta(\zeta) \approx \frac{C_\theta h\theta_{*\rm s}}{k_T L_{\rm s}}\Phi_\theta(\zeta), \tag{53}$$

where $\Phi_\theta = \int_\zeta^1 f_\theta(\zeta)\,{\rm d}\zeta$. The approximate expression on the r.h.s. of Eq. (53) is justified when the capping inversion layer is comparatively shallow: $\frac{1}{2}\delta_{\rm CI} \ll h$.

Considering Eq. (53) in the $z$-less stratification part of the surface layer and substituting the lower line of Eq. (51) for $\theta(z)$ on the l.h.s. of Eq. (53) yields:

$$k_T\frac{\theta_{h-0} - \theta_0}{\theta_{*\rm s}} - \ln\frac{L_{\rm s}}{C_\theta z_{0u}} - 1 = C_\theta\frac{h}{L_{\rm s}}\{\zeta + \Phi_\theta(\zeta)\} = c\frac{h}{L_{\rm s}} \quad (c = \text{constant}). \tag{54}$$

The r.h.s. of Eq. (54) is simply a universal constant (assigned $c$) because the l.h.s. of this equation does not depend on $z$.

Equation (54) is consistent with the temperature-resistance law, Eq. (8) (provided that the temperature increment across the PBL is defined after Eq. (47)) and implies the following asymptotic expression of the coefficient $C$ at $h/L_{\rm s} \gg 1$:

$$C = -c(h/L_{\rm s}) + \ln(h/L_{\rm s}) + \ln C_\theta + 1 = -c(h/L_{\rm s}) + \ln(h/L_{\rm s}) + \text{constant}. \tag{55}$$

Employing the same approach as in section 2(c), Eq. (55) is extended to include both the near-neutral and the long-lived stable PBLs:

$$C = -cm_C + \ln(\exp(c_0) + m_C) \approx c_0 - cm_C, \tag{56}$$

where $m_C$ is a composite stratification parameter:

$$m_C = \left\{ \left(\frac{h}{L_s}\right)^2 + \left(\frac{C_{NC}h}{L_N}\right)^2 + \left(\frac{C_{fC}h}{L_f}\right)^2 \right\}^{1/2}. \tag{57}$$

$C_{NC}$, $C_{fC}$, $c$ and $c_0$ are dimensionless constants of the same type as the constants in Eqs. (42) and (43).

LES data shown in Fig. 6 confirm Eqs. (56), (57) with reasonable accuracy and give estimates of the dimensionless constants $C_{NC} = 1.2$, $C_{fC} = 1$, $c = 4.1$ and $c_0 = 12$. The large value of $c_0$ justifies the approximate version of Eq. (56). Equations (5), (8), (12), (56) and (57) comprise the heat-transfer law.

In the near-neutral steady-state PBL (when $h \to h_E = C_R u_*/|f|$), the stratification parameter $m_C$ and the potential-temperature resistance-law coefficient $C$ approach limits: $m_C \to C_{fC}C_R$ =0.7 and $C \to C_0 = c_0 - cC_{fC}C_R = 9.1$. Typically, in the stratified PBLs, $m_C > 0.7$; but $m_C$ could be less than the above limit in shallow evolving PBLs.

Recall that the baroclinic versions of the turbulent-length scale and the equilibrium PBL depth are $L_N = u_T/N$, and $h_E \sim u_T(|f|N)^{-1/2}$, where $u_T$ in given by Eq. (11). Hence the effect of baroclinicity on the ratio $h/L_N$ can be neglected, at least as a first approximation (cf. the same conclusion in the discussion of Eq. (39) at the end of subsection 2(c)).

## 3. LARGE-EDDY SIMULATIONS

In this paper we systematically use data from numerical simulations based on a new LES code (Esau 2004a). This code solves the momentum, temperature and continuity equations for an incompressible Boussinesq fluid:

$$\frac{\partial u_i}{\partial t} = -\frac{1}{2}u_j\frac{\partial u_i}{\partial x_j} - \frac{\partial}{\partial x_j}\left(\frac{1}{2}u_iu_j + p\delta_{ij} + \tau_{ij}\right) - f\omega_j - \frac{g}{T_0}\Theta\delta_{i3}, \tag{58}$$

and

$$\frac{\partial \Theta}{\partial t} = -\frac{\partial}{\partial x_j}(u_j\Theta + \tau_{\Theta j}), \quad \frac{\partial u_i}{\partial x_i} = 0. \tag{59}$$

Here, $u_i = \{u, v, w\}$, $\Theta$, $p$ are large-scale velocity, potential temperature and pressure; $\tau_{ij}$, $\tau_{\Theta j}$ are subgrid-scale turbulence stress and temperature flux tensors; $f\omega_j = \{f(v_g - v - w \cdot \cot\varphi),\ f(-u_g + u),\ fu \cdot \cot\varphi)\}$ are the components of the Coriolis force; $\varphi$ is the latitude; $\delta_{ij} = 1$ at $i = j$ and $\delta_{ij} = 0$ at $i \neq j$; the repeating indices imply summation.

The code uses the fully conservative second order central-difference scheme (Morinishi *et al.* 1998) for advection, and the fourth order Runge-Kutta scheme (Jameson *et al.* 1981) for time stepping. The direct fractional-step pressure correction scheme (Armfield and Street 1999) ensures incompressibility in the code. This set of numerical schemes is a kind of standard in computational fluid dynamics. Moreover, Andren *et al.* (1994) concluded that differences in numerical schemes have a minor effect on LES results. Later, Brown *et al.* (2000) reported that LES results are encouragingly insensitive to the choice of numerical schemes, as long as simulations resolve some part of the inertial sub-range of scales. The computational mesh is the staggered C-type.

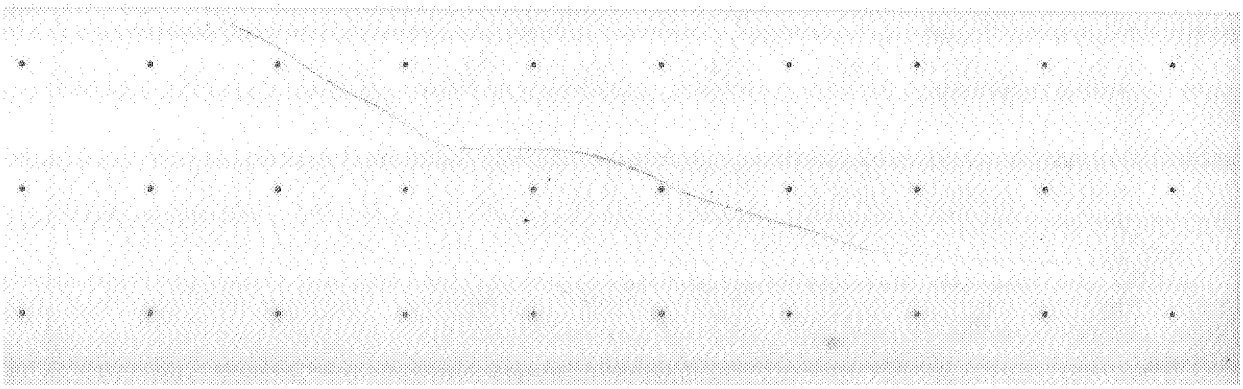

The grid spacing is uniform and almost isotropic. The horizontal grid size $\Delta_x$, is larger than the vertical grid size $\Delta_z$, but their ratio $\Delta_x/\Delta_z$ is always less than four.

An important part of the LES technique is a subgrid turbulence closure. This LES code employs a dynamic mixed closure (Vreman *et al.* 1994):

$$\tau_{ij} = \{\overline{(u_i u_j)} - (\overline{u_i})\,(\overline{u_j})\} + \{-2l_s^2|S_{ij}|S_{ij}\}, \tag{60a}$$

$$S_{ij} = \frac{1}{2}\left(\frac{\partial u_i}{\partial x_j} + \frac{\partial u_j}{\partial x_i}\right), \tag{60b}$$

$$\tau_{\Theta j} = -2\,\mathrm{Pr}_t^{-1}\, l_s^2 |S_{ij}| \frac{\partial \Theta}{\partial x_j}, \tag{61}$$

where, $\mathrm{Pr}_t$ is an empirical turbulent Prandtl number taken after Kondo *et al.* (1978).

The first term $\{\overline{(u_i u_j)} - (\overline{u_i})\,(\overline{u_j})\}$ represents the direct dissipation of energy in nonlinear interactions of large eddies. The filter (denoted by overbar) determines the scale interval in which this direct energy dissipation is possible. In the present LES code the interval has the size of two grid cells. This term was not included in prior environmental LES codes; its importance has been recognized only recently through analyses of data from atmospheric field experiments (Sullivan *et al.* 2003).

The second term $-2l_s^2|S_{ij}|S_{ij}$ in Eq.(60a) and the term $-2\,\mathrm{Pr}_t^{-1}\, l_s^2|S_{ij}|(\partial\Theta/\partial x_j)$ in Eq. (61) represent a Smagorinsky type of eddy viscosity closure (Smagorinsky 1963). It parametrizes local and instant energy dissipation by small eddies through numerical solution of a variation problem for the mixing-length scale $l_s(x_i, t)$ at every time step. Comparative tests of this LES code are presented by Esau (2004a).

It is worth mentioning that advantages of the dynamic mixed closure become important only in the case of strong flow anisotropy or very strong static stability. Both cases are actually equivalent since the strong static stability increases the eddy anisotropy. In these cases the first term in Eq. (60a) becomes large or even dominant. Most of the LES runs in our database correspond to moderate flow anisotropy and static stability, thus the subgrid turbulence closure should not be considered as a critical component of the present study.

The design of all LES runs followed a standard scheme. The LES domain had 64 grid points in each direction. Chapman (1978) provided the following criterion of a well-resolved boundary-layer flow: 15–30 computational levels within the PBL; we followed this criterion. The PBL always comprised about 1/2 to 2/3 of the LES domain. Accordingly, the physical resolution varied from about 0.5 m (for very stable PBL runs) to more than 50 m (for truly neutral PBL runs).

Figure 7 shows the quality of the LES in terms of the ratio $Q_E$ of the subgrid turbulent kinetic energy (TKE) to the resolved TKE: $Q_E = \int_0^h E^{SGS}\,dz / \int_0^h E^{RES}\,dz$, presented as dependent on the dimensionless resolution $\Delta_z/L_M$, where $\Delta_z$ is the vertical grid size, and $L_M$ is the turbulent-length scale. Clearly, both ratios $Q_E$ and $\Delta_z/L_M$ should be small in a well-resolved LES. Our LES runs satisfied the conditions $Q_E < 1/4$ and $\Delta_z/L_M < 1$, which gives grounds to expect that the subgrid-scale effects were negligible.

The upper-boundary conditions are of von Neumann type, or stressless rigid lid, $\nabla_z u_i = \nabla_z \Theta = \nabla_z p = 0$, $w = 0$.

The lower-boundary conditions are:

- Prescribed subgrid-scale turbulent flux of potential temperature $\tau_{\Theta j}$;
- Logarithmic wall law: $\tau_{i3} = \{\kappa|u_i(z = \Delta_z/2)|/\ln(\Delta_z/2z_0)\}^2$, $\tau_{i1} = \tau_{i2} = 0$, where $\Delta_z/2$ is the height of the first computational level.

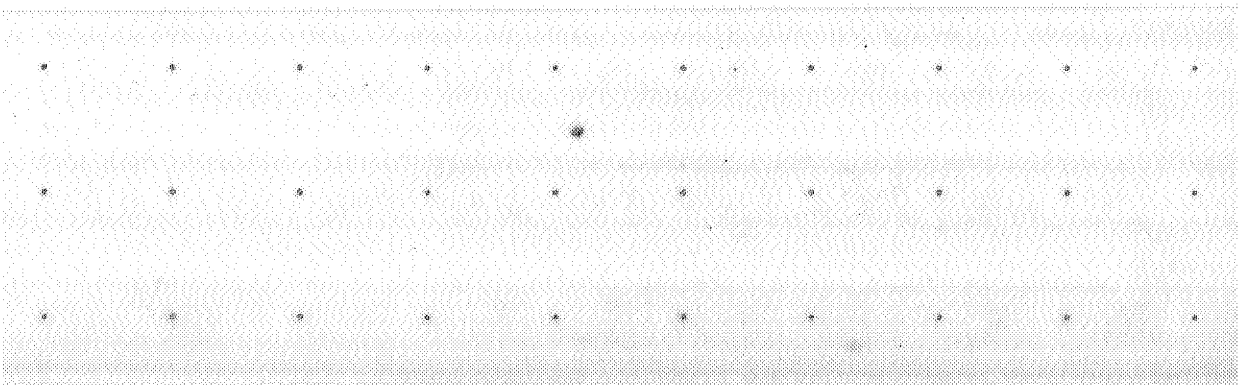

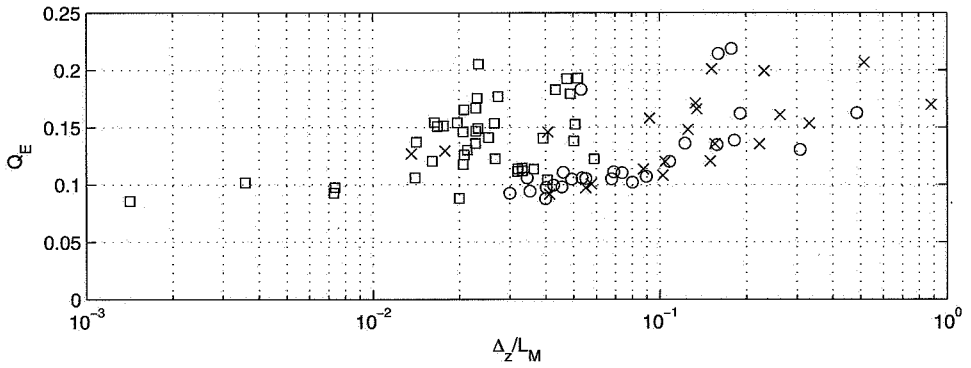


Figure 7. The ratio $Q_E = \int_0^h E^{SGS}\,dz / \int_0^h E^{RES}\,dz$ of the subgrid to the resolved portions of the turbulent kinetic energy as dependent on the dimensionless vertical resolution $\Delta_z/L_M$. The smaller $Q_E$ and $\Delta_z/L_M$ are, the higher is the quality of the large-eddy simulation run. See text for further details.

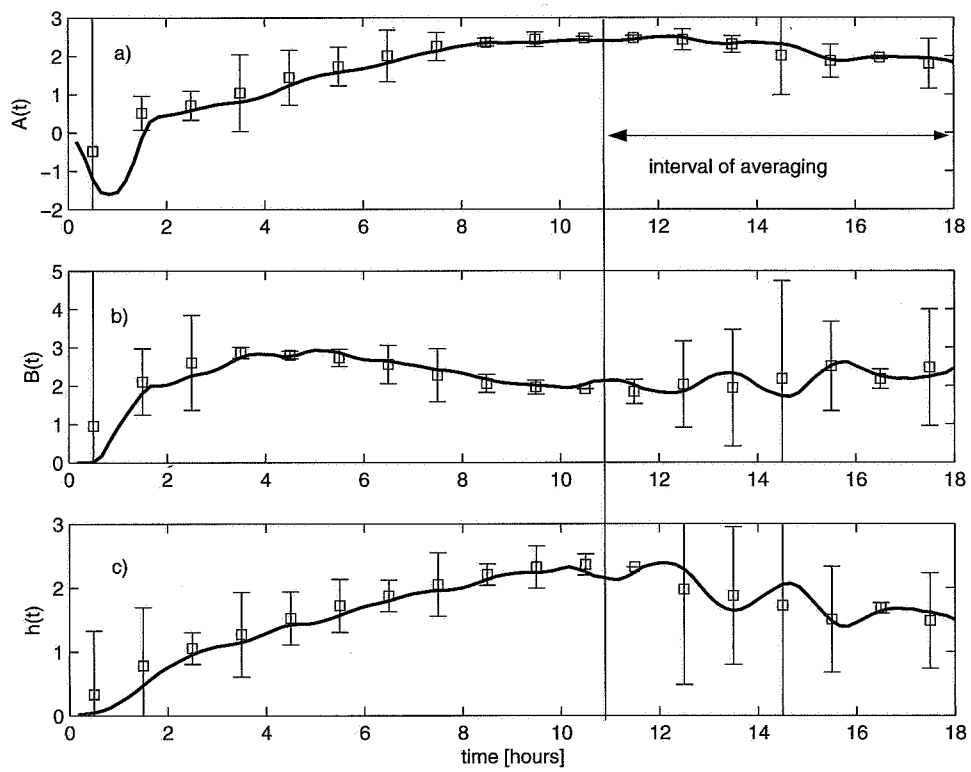


Figure 8. Temporal evolution of the resistance-law coefficients $A_0$, $B_0$, and the planetary boundary layer (PBL) depth $h_{PBL}$, in the large-eddy simulation (LES)-generated truly neutral PBL ($G = 5$ m s$^{-1}$, $z_{0u} = 0.1$ m, $f = 10^{-4}$ s$^{-1}$, $F_{\theta s} = 0$, $N = 0$). Squares show mean values averaged over 1 h intervals. Error bars show the $\pm 3$ standard deviation intervals for each hour. The solid line shows filtered 10-minute data. See text for further details.

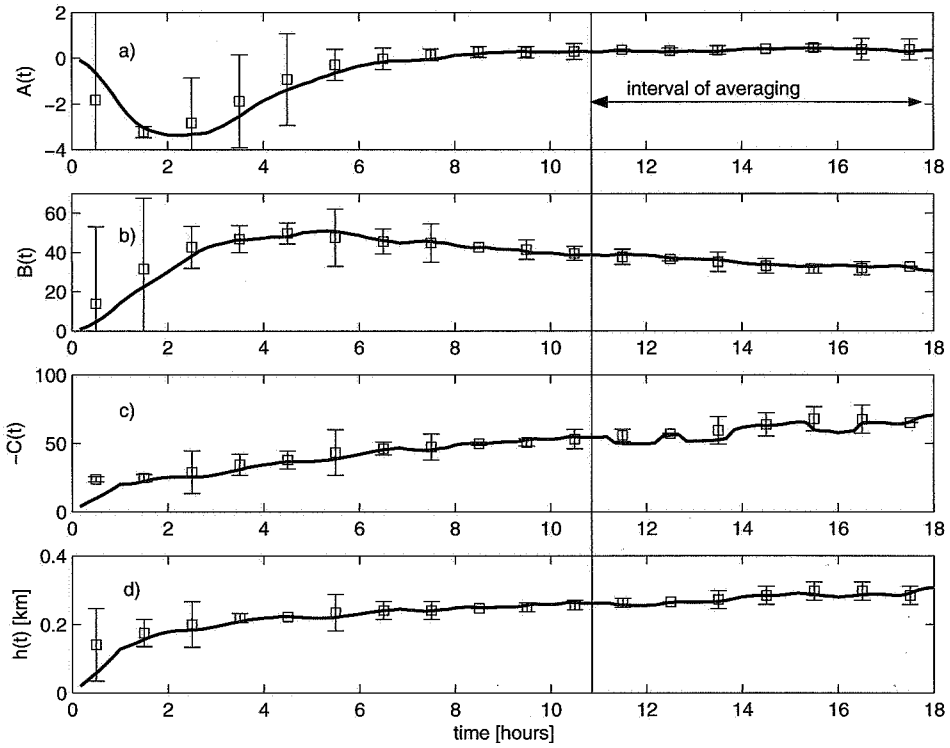


Figure 9. Same as in Fig. 8, but for the resistance-law coefficients $A$, $B$, $C$ and the PBL depth $h_{\mathrm{PBL}}$ in the LES-generated long-lived stable PBL ($G = 5$ m s$^{-1}$, $z_{0u} = 0.1$ m, $f = 10^{-4}$ s$^{-1}$, $F_{\theta s} = 0.005$ K m s$^{-1}$, $N = 0.01$ s$^{-1}$). See text for details.

The initial mean profiles are specified as linearly increasing potential temperature (a prescribed depth-constant temperature gradient) and a prescribed depth-constant wind velocity at all levels down to the surface. The initial flow is laminar with imposed very small random perturbations at the first three to five computational levels. The initial profiles, perturbations, surface fluxes and the Coriolis force are not adjusted to each other; hence every run goes through a spin-up phase. During this period (usually 3–5 model hours) all turbulence characteristics are statistically unsteady. As an example, Figs. 8 and 9 show the temporal evolution of the $A$, $B$ and $C$ coefficients in the truly neutral and the long-lived stable PBL runs.

The typical run duration is 64800 s (18 model hours). We accept that the basic characteristics of turbulence reach steady state in the last 7 model hours. Averaging over this time interval is used to create the database.

To account for the residual, long-term variations of turbulent characteristics, we (probably for the first time in LES practice) calculated and plotted not only the mean values of the modelled parameters (in particular the $A$, $B$ and $C$ coefficients) but also their standard deviations. These residual variations are partially caused by incomplete achievement of the steady state. This effect is especially pronounced for such sensitive parameters as the cross-isobaric angle, $\alpha$ (therefore the $B$ coefficient) and the temperature increment across the proper PBL, $\Delta\theta_{\mathrm{PBL}}$ (therefore the $C$ coefficient). It causes the rather large scatter of data points in Figs. 4 and 6. In very stable PBLs, the scatter could also be caused by the turbulence intermittency (Mahrt 1985).

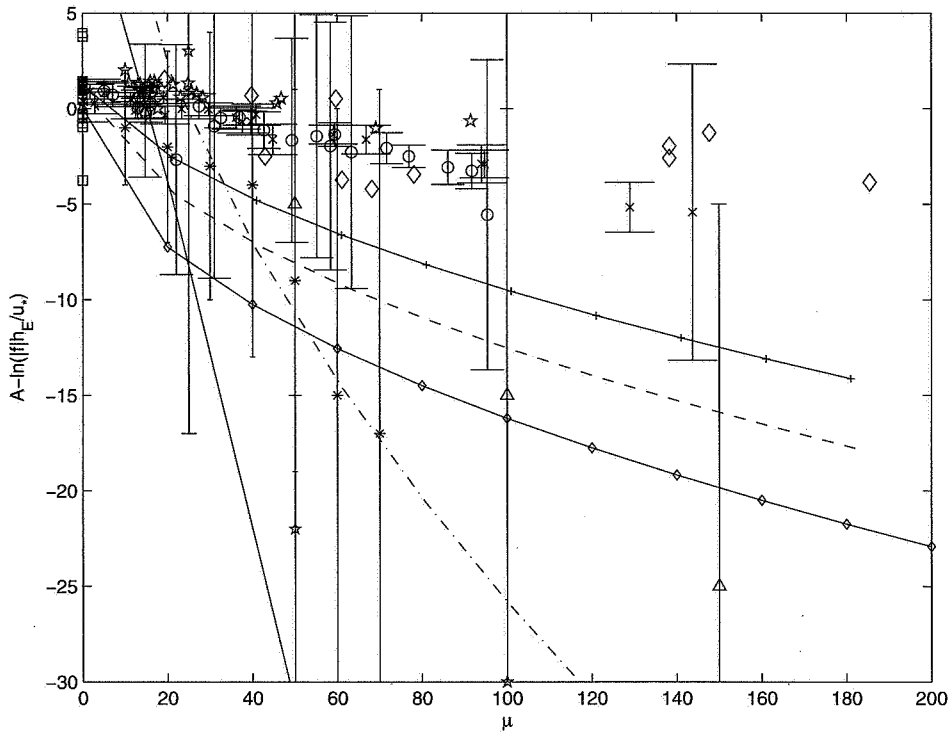


Figure 10. Traditional presentation of the geostrophic-drag resistance-law coefficient $\widetilde{A} \equiv A - \ln(|f|h_E/u_*)$ as a single-valued function of the internal stability parameter $\mu = u_*/|f|L$. Data points are taken from different sources: points shown as crosses, circles and squares are new large-eddy simulation (LES) data for the nocturnal, long-lived and conventionally neutral planetary boundary layers, respectively; points shown as diamonds and stars represent earlier LES data from Brown *et al.* (1994) and Kosovic and Curry (2000), respectively. Other symbols are field data: asterisks—Cabauw (Nieuwstadt 1981), triangles—Wangara (Yamada 1976), plus signs—different Russian sites (Zilitinkevich and Chalikov 1968). The curves show old analytical approximations (summarized by Byun 1991): full line—Vachat and Musson-Genon, dashed line—Arya, dash-dotted line—Long and Guffey, line with plus signs—Brost and Wyngaard, and the line with diamonds—Derbyshire. Error bars show the ±3 standard deviation intervals. See text for further details.

## 4. VERIFICATION OF RESISTANCE AND HEAT-TRANSFER LAWS AGAINST LES DATA

Earlier atmospheric measurements gave very uncertain estimates of the $\widetilde{A}$, $\widetilde{B}$ and $\widetilde{C}$ (or $A$, $B$ and $C$) coefficients, which are considered—according to the theoretical expectations of the time—as single-valued functions of $\mu = u_*/|f|L_s$ (or $h/L_s$). Although data from particular field-experiment programmes, such as Cabauw (Nieuwstadt 1981) or Wangara (Yamada 1976), could show reasonable collapses, data summaries including results from different experimental sites always exhibited enormously huge scatter (e.g. Zilitinkevich and Chalikov 1968; Zilitinkevich 1975). Besides insufficient accuracy of earlier experiments, this huge scatter could to some extent be caused by the newly recognized effects, namely the free-flow stability, baroclinicity and deviations from the equilibrium state, overlooked in the prior resistance and heat-transfer formulations.

As illustrations, Figs. 10–12 present the $\widetilde{A}$, $\widetilde{B}$ and $\widetilde{C}$ coefficients in the traditional way—as functions of $\mu$, combining data from earlier atmospheric measurements, earlier LES and a new LES database. In this old format, the earlier and the new LES data, although they showed reasonably good results in Figs. 3, 4 and 6, only added to the scatter.

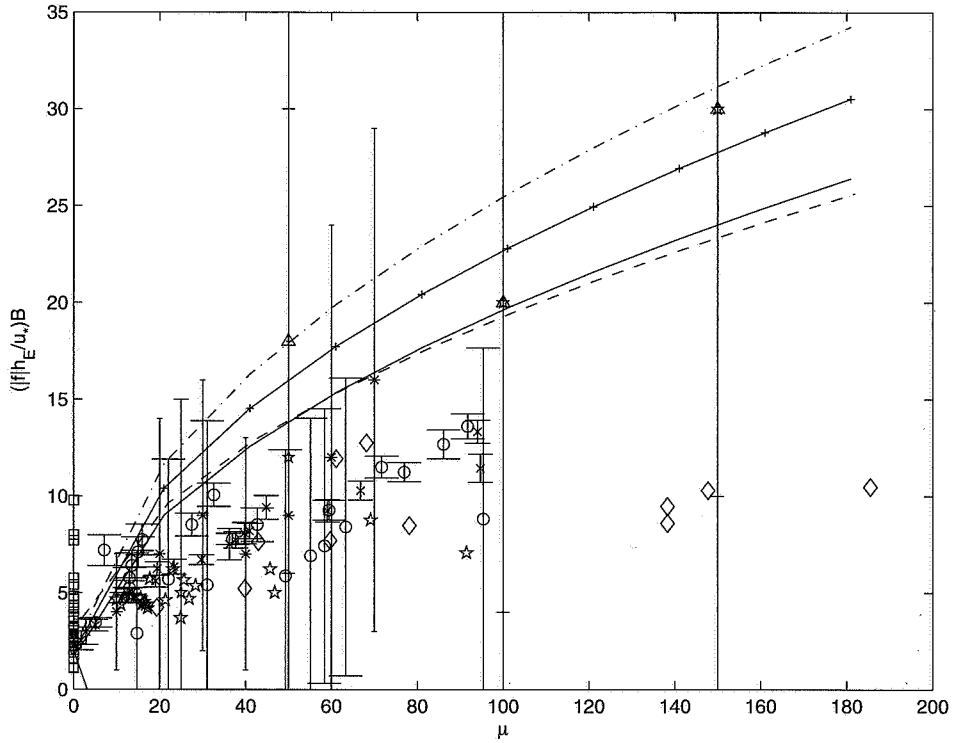


Figure 11. Same as in Fig. 10, but for the cross-isobaric-angle resistance-law coefficient $\widetilde{B}(\mu) \equiv (|f|h_{\mathrm{E}}/u_*)B$.

It is not surprising that old analytical approximations for $\widetilde{A}(\mu)$, $\widetilde{B}(\mu)$ and $\widetilde{C}(\mu)$ taken from Byun (1991) reflect this scatter and look rather chaotic. Unfortunately the earlier atmospheric data did not include sufficient information to enable them to be presented in the new format. In any event, the striking difference between Figs. 10–12 based on the old theory and Figs. 3, 4 and 6 based on the advanced theory catches the eye.

The advantage of new theory is very clearly seen in the weak- and moderate-stability regimes. Indeed, the traditional type of functions $\widetilde{A}(\mu)$, $\widetilde{B}(\mu)$ and $\widetilde{C}(\mu)$ exhibit incomparably larger scatter at small values of the internal stability parameter, $\mu$, than the new functions $A(m_A)$, $B(m_B)$ and $C(m_C)$ at small values of the composite stability parameters $m_A$, $m_B$ and $m_C$. Pronounced scatter of data on $C(m_C)$ at very small $m_C$ is not surprising because small values of $m_C$ imply very small temperature fluxes and temperature increments across the PBL, which inevitably result in considerable errors in the estimates of $\theta_*$, $\Delta\theta_{\mathrm{PBL}}$ and $m_C$.

## 5. Conclusions

In the traditional context, the terms 'stably stratified atmospheric PBL' and 'nocturnal PBL' were considered as synonyms, whereas the term 'neutrally stratified PBL' was applied to all PBLs characterized by the zero buoyancy flux at the surface ($F_{\theta \mathrm{s}} = 0$) without any regard to the Brunt–Väisälä frequency, $N$, in the free atmosphere above the PBL. In contrast, we distinguish between the following essentially different types of stable PBLs:

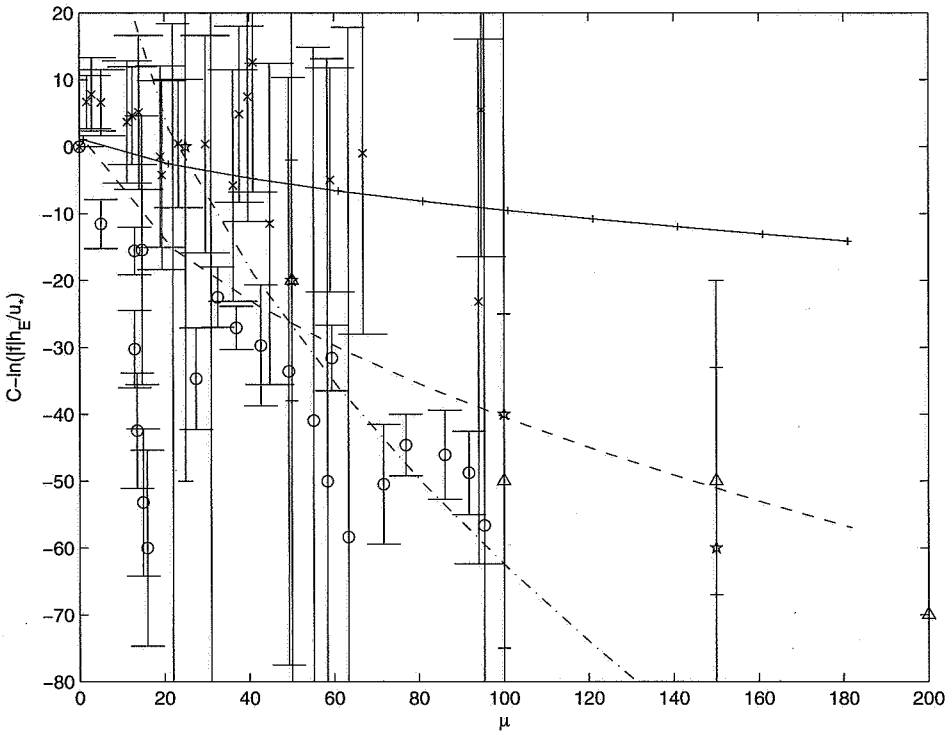


Figure 12. Same as in Figs. 10 and 11, but for the temperature resistance-law coefficient $\widetilde{C}(\mu) \equiv C - \ln(|f|h_E/u_*)$.

• *Short-lived* PBLs, namely, the nocturnal stable ($F_{\theta s} < 0$, $N = 0$) and the truly neutral ($F_{\theta s} = 0$, $N = 0$) PBLs that develop against neutrally stratified residual layers. They exhibit basically local nature. In these regimes, the Monin–Obukhov similarity theory realistically describes the surface-layer turbulence.

• *Long-lived* PBLs, namely, the thoroughly stable ($F_{\theta s} < 0$, $N > 0$) and the conventionally neutral ($F_{\theta s} = 0$, $N > 0$) PBLs that develop over a sufficiently long period to approach the stably stratified free atmosphere. Their basic features (including the surface-layer scaling) are essentially controlled by the non-local effect of $N$. In these regimes, the classical similarity theory is no longer applicable; besides the familiar Monin–Obukhov length scale $L$, an important role is played by the external stability scale $L_N = u_*/N$.

At $N = 0$, the effect of baroclinicity would result in making the overall troposphere turbulent. It is not surprising that the traditional models of short-lived PBLs did not account for this effect. On the contrary, additional mixing due to the baroclinic shear ($\Gamma$) is very naturally included in the long-lived-PBL model through the baroclinic turbulent-velocity scale $u_T = u_*(1 + C_b\Gamma/N)^{1/2}$.

In the present paper, the resistance and heat-transfer laws are advanced, covering non-steady PBLs and accounting for the effect of $N$, both of which were disregarded in prior models and are now reflected through the composite stratification parameters $m_A$, $m_B$ and $m_C$, see Eqs. (42), (43) and (57), whereas the effect of $\Gamma$ is included through the baroclinic PBL-depth formulation (Zilitinkevich and Esau 2003).

In contrast to prior formulations, the newly derived resistance-law formula for the cross-isobaric angle, Eq. (7b), explicitly shows the role of the Coriolis parameter $f$.

The proposed theory sheds light on the cause of a very wide spread of data in prior empirical graphs presenting the resistance-law coefficients as single-valued functions of a sole stratification parameter, such as $\mu = u_*/|f|L_s$ or $h/L_s$. It is shown that this spread was to a large extent caused by effects unaccounted for in the traditional context. Analogous graphs based on the new theory show much better correspondence with data.

The resistance and heat-transfer laws given by Eqs. (5), (7), (8), (41) to (43), (56) and (57) provide the physical background for an advanced surface-flux calculation scheme applicable to a wide range of PBLs including very shallow boundary layers. Such a scheme would respond to the urgent demand from operational modellers. Indeed, all currently used surface-flux schemes are based on the concept of 'the surface layer', which implies that the turbulent fluxes are taken to be depth-constant ($\tau = u_*^2$, $F_\theta = F_{\theta s}$) from the surface $z = 0$, up to the lowest computational level $z = z_1$. Clearly, this assumption is justified only when the PBL height, $h$, is an order of magnitude larger than $z_1$. However, in operational models $z_1$ must not be taken too small (in particular, $z_1$ is close to 30 m in the most advanced numerical weather prediction and climate models: ECMWF†, HIRLAM‡, ECHAM§, etc.). At the same time, as recognized recently, the typical height of long-lived stable PBLs is just a few dozen metres (Zilitinkevich and Esau 2003). Traditional surface-flux schemes completely fail in such cases (see Esau 2004b) so there is simply no alternative to an approach based on resistance laws.

New advancement of the resistance and heat-transfer laws makes them principally applicable to the oceanic upper and bottom boundary layers. Notice that the role of the external stability parameter $\mu_N$, Eq. (10a), is absolutely dominant in the upper layer of water, because of the very strong static stability typically observed in the thermocline below the PBL. It is conceivable that the advanced laws—reformulated and validated against oceanographic data—can be used as the physical basis for improved calculations of the key parameters characterizing the oceanic boundary layers: turbulent fluxes of momentum and scalars at the ocean bottom; velocity and direction of the surface-drift currents; increments in the temperature, salinity and other scalar admixtures across thin films at the water surface (see Zilitinkevich and Kreiman 1991). Such calculations are required in a number of practical problems, such as the modelling of $CO_2$ exchanges between the atmosphere and the ocean, and modelling the transport and dispersion of oil films at the water surface.

LES data analyses performed here to support our background assumptions and to validate final results (and LES database as such) could be of interest beyond this research. In particular, they confirm well-pronounced self-similarity of normalized turbulent-flux profiles (Fig. 1) and reveal feasibility of the generalized scaling based on Eq. (14) for all kinds of stable PBLs (Figs. 2 and 5).

## ACKNOWLEDGEMENTS

This work has been supported by the EU Marie Curie Chair Project MEXC-CT-2003-509742; ARO Project 'Advanced Parameterization and modelling of turbulent atmospheric boundary layers'—contract number W911NF-05-1-0055; EU Project FUMAPEX EVK4-2001-00281; Norwegian project MACESIZ 155945/700; and joint Norwegian-USA project ROLARC 151456/720. This work was partially carried out

† European Centre for Medium-Range Forecasts.

‡ High Resolution Limited-Area Model.

§ ECMWF model HAMburg version.

while SSZ was visiting the Institute for Mathematical Sciences, National University of Singapore in 2004 (this visit was supported by the Institute). The authors thank Dale Hess and Sylvain Joffre for valuable comments.

## APPENDIX

### *Self-similarity of the vertical profile of the momentum flux*

In the nocturnal PBLs, the assumption of self-similarity of the vertical turbulent flux of momentum is consistent with the following scaling analysis of the Ekman equations. Taking $\tau/u_*^2 = f_\tau(\zeta)$ and $F_\theta/F_{\theta s} = f_{F\theta}(\zeta)$, the approximate eddy-viscosity formulation, Eq. (16), becomes $K_M = K_M^* f_{KM}(\zeta)$, where $K_M^* = kC_u^{-1}u_* L_s$ is a depth-constant eddy-viscosity scale and $f_{KM}(\zeta) = f_\tau^2 f_{F\theta}^{-1}$ is a universal function decreeing towards the PBL upper boundary (our LES-based analytical approximations give $f_{KM} = \exp(-10\zeta^2/3)$). Then, differentiating Eq. (25) over $z$, multiplying by $K_M$, using the PBL height-scale $h \sim (K_M^*/|f|)^{1/2}$ and going to dimensionless variables $\zeta = z/h$ and $\widehat{\tau}_{\{x,y\}} = \tau_{\{x,y\}}/u_*^2$, yields:

$$\widehat{\tau}_y + f_{KM}(\zeta)\frac{\partial \widehat{\tau}_x}{\partial \zeta} = 0, \quad -\widehat{\tau}_x + f_{KM}(\zeta)\frac{\partial \widehat{\tau}_y}{\partial \zeta} = 0.$$

The boundary conditions, Eq. (26), take the form $\widehat{\tau}_x = 1$, $\widehat{\tau}_y = 0$ at $\zeta = 0$ and $\widehat{\tau}_x = 0$, $\widehat{\tau}_y = 0$ at $\zeta \to \infty$. Thus the problem becomes self-similar, which ensures that $\widehat{\tau}_x$ and $\widehat{\tau}_y$ are single-valued functions of $\zeta$. Figure 1 confirms this conclusion and gives grounds to extend it to long-lived and conventionally neural PBLs.

## REFERENCES


Andren, A., Brown, A. R., Graf, J., Mason, P. J., Moeng, C.-H., Nieuwstadt, F. T. N. and Schumann, U. 1994 Large-eddy simulation of a neutrally stratified layer: A comparison of four computer codes. *Q. J. R. Meteorol. Soc.*, **120,** 1457–1484

Armfield, S. and Street, R. 1999 The fractional step method for the Navier–Stokes equations on staggered grids: The accuracy of three variations. *J. Comput. Phys.*, **153,** 660–665

Arya, S. P. S. 1975 Comments on 'Similarity theory for the planetary boundary layer of time-dependent height'. *J. Atmos. Sci.*, **32,** 839–840

Arya, S. P. S. and Wyngaard, J. C. 1975 Effect of baroclinicity on wind profiles and the geostrophic drag law for the convective planetary boundary layer. *J. Atmos. Sci.*, **32,** 767–778

Brown, A. R., Derbishire, S. H. and Mason, P. J. 1994 Large-eddy simulation of stable atmospheric boundary layers with a revisited stochastic backscatter subgrid model. *Q. J. R. Meteorol. Soc.*, **120,** 1485–1512

Brown, A. R., MacVean, M. K. and Mason, P. J. 2000 The effects of numerical dissipation in large eddy simulations. *J. Atmos. Sci.*, **57,** 3337–3348

Byun, D. 1991 Determination of similarity functions of the resistance laws for the planetary boundary layer using surface layer similarity functions. *Boundary-Layer Meteorol.*, **57,** 17–48

Chapman, D. R. 1978 Computational aerodynamics, development and outlook. *AIAA J.*, **17**(12), 1293–1313

Csanady, G. T. 1974 Equilibrium theory of the planetary boundary layer with an inversion lid. *Boundary-layer Meteorol.*, **6,** 63–79

Djolov, G., Yordanov, D. and Syrakov, D. 2004 Baroclinic planetary boundary layer model for neutral and stable stratification conditions. *Boundary Layer Meteorol.*, **111,** 467–490

Esau, I. N. 2004a Simulation of Ekman boundary layers by a large eddy model with dynamic mixed sub-filter closure. *Environ. Fluid Mech.*, **4,** 273–303

Esau, I. N. 2004b Parameterization of a surface drag coefficient in a conventionally neutral planetary boundary layer. *Annales Geophysicae*. **22,** 3353–3362

Garratt, J. R. 1992 *The atmospheric boundary layer*. Cambridge University Press, London, UK

Gill, A. E. 1968 Similarity theory and geostrophic adjustment. *Q. J. R. Meteorol. Soc.*, **94,** 586–588

Hess, G. D. 2004 The neutral, barotropic planetary boundary layer, capped by a low-level inversion. *Boundary-Layer Meteorol.*, **110,** 319–355

Hess, G. D. and Garratt, J. R. 2002a Evaluating models of the neutral, barotropic planetary boundary layer using integral measures. Part I: Overview. *Boundary-Layer Meteorol.*, **104,** 333–358

2002b Evaluating models of the neutral, barotropic planetary boundary layer using integral measures. Part II: Modelling observed conditions. *Boundary-Layer Meteorol.*, **104,** 359–369

Jameson, A., Schmidt, W. and Turkel, E. 1981 Numerical simulation of the Euler equations by finite volume methods using Runge-Kutta time stepping schemes. *AIAA Paper* **81,** 1259

Joffre, S. M. 1982 Assessment of separate effects of baroclinicity and thermal stability in the atmospheric boundary layer over the sea. *Tellus*, **34,** 567–578

1984 Effects of local accelerations and baroclinicity on the mean structure of the atmospheric boundary layer over the sea. *Boundary-Layer Meteorol.*, **32,** 237–255

Kazanski, A. B. and Monin, A. S. 1961 On turbulent regime above the surface layer. *Izvestija AN SSSR Geophysical Series*, No. 1, 165–168

King, J. and Turner, J. 1997 *Antarctic meteorology and climatology*. Cambridge University Press, London, UK

Kitaigorodskii, S. A. and Joffre, S. M. 1988 In search of simple scaling for the heights of the stratified atmospheric boundary layer. *Tellus*, **40A,** 419–443

Kondo, J., Konechika, O. and Yasuda, N. 1978 Heat and momentum transfer under strong stability in the atmospheric surface layer. *J. Atmos. Sci.*, **35,** 1012–1021

Kosovic, B. and Curry, J. 2000 A large eddy simulation study of a quasi-steady, stably stratified atmospheric boundary layer. *J. Atmos. Sci.*, **57,** 1052–1068

Lenschow, D. H., Li, X. S., Zhu, C. J. and Stankov, B. B. 1988 The stably stratified boundary layer over the Great Plains. Part 1: Mean and turbulence structure. *Boundary-layer Meteorol.*, **42,** 95–121

Mahrt, L. 1985 Vertical structure and turbulence in the very stable boundary layer. *J. Atmos. Sci.*, **42,** 2333–2349

Mahrt, L. and Vickers, D. 2002 Contrasting vertical structures of nocturnal boundary layers. *Boundary Layer Meteorol.*, **105,** 351–363

Mason, P. J. 1994 Large-eddy simulation: A critical review of the technique. *Q. J. R. Meteorol. Soc.*, **120,** 1–26

Monin, A. S. and Obukhov, A. M. 1954 Main characteristics of the turbulent mixing in the atmospheric surface layer. *Trudy Geophys. Inst. AN. SSSR*, **24**(151), 153–187

Morinishi, Y., Lund, T. S., Vasiljev, O. V. and Moin, P. 1998 Fully conservative higher order finite difference schemes for incompressible flow. *J. Comput. Phys.*, **143,** 90–124

Nieuwstadt, F. T. M. 1981 The steady-state height and resistance laws of the nocturnal boundary layer: Theory compared with Cabauw observations. *Boundary-Layer Meteorol.*, **20,** 3–17

1984 The turbulent structure of the stable nocturnal boundary layer. *J. Atmos. Sci.*, **41,** 2202–2216

Overland, J. E. and Davidson, K. L. 1992 Geostrophic drag coefficient over sea ice. *Tellus*, **44A,** 54–66

Rossby, C. G. and Montgomery, R. B. 1935 The layers of frictional influence in wind and ocean currents. *Pap. Phys. Oceanogr. Meteorol.*, **3**(3), 101 pp.

Smagorinsky, J. 1963 General circulation experiments with the primitive equations. *Mon. Weather Rev.*, **91**(3), 99–164

Sodemann, H. and Foken, T. 2004 Empirical evaluation of an extended similarity theory for the stably stratified atmospheric surface layer. *Q. J. R. Meteorol. Soc.*, **130,** 2665–2671

Sorbjan, Z. 1988 Structure of the stably-stratified boundary layer during the SESAME-1979 experiment. *Boundary-Layer Meteorol.*, **44,** 255–266

Sullivan, P. P., Horst, Th. W., Lenschow, D. H., Moeng, C.-H. and Weil, J. C. 2003 Structure of subfilter-scale fluxes in the atmospheric surface layer with application to large-eddy simulation modelling. *J. Fluid Mech.*, **482,** 101–139

Tjenstroem, M. and Smedman, A.-S. 1993 The vertical structure of the coastal marine atmospheric boundary layer. *J. Geophys. Res.*, **98**(C3), 4809–4826

Vreman, B., Geurts, B. and Kuerten, H. 1994 On the formulation of the dynamic mixed subgrid-scale model. *Phys. Fluids*, **6**(12), 4057–4059

Wittich, K. P. 1991 The nocturnal boundary layer over northern Germany: An observational study. *Boundary-Layer Meteorol.*, **55,** 47–66

Yamada, T. 1976 On similarity functions A, B and C of the planetary boundary layer. *J. Atmos. Sci.*, **33,** 781–793

Zilitinkevich, S. 2002 Third-order transport due to internal waves and non-local turbulence in the stably stratified surface layer. *Q. J. R. Meteorol. Soc.*, **128,** 913–925

Zilitinkevich, S. and Calanca, P. 2000 An extended similarity-theory for the stably stratified atmospheric surface layer. *Q. J. R. Meteorol. Soc.*, **126,** 1913–1923

Zilitinkevich, S., Johansson, P.-E., Mironov, D. V. and Baklanov, A. 1998 A similarity-theory model for wind profile and resistance law in stably stratified planetary boundary layers. *J. Wind Eng. Industr. Aerodyn.*, **74–76,** 209–218

Zilitinkevich, S., Baklanov, A., Rost, J., Smedman, A.-S., Lykosov, V. and Calanca, P. 2002 Diagnostic and prognostic equations for the depth of the stably stratified Ekman boundary layer. *Q. J. R. Meteorol. Soc.*, **128,** 25–46

Zilitinkevich, S. S. 1972 On the determination of the height of the Ekman boundary layer. *Boundary-Layer Meteorol.*, **3,** 141–145

1975 Resistance laws and prediction equations for the depth of the planetary boundary layer. *J. Atmos. Sci.*, **32,** 741–752

1989 Velocity profiles, resistance law and the dissipation rate of mean flow kinetic energy in a neutrally and stably stratified planetary boundary layer. *Boundary-Layer Meteorol.*, **46,** 367–387

Zilitinkevich, S. S. and Baklanov, A. 2002 Calculation of the height of stable boundary layers in practical applications. *Boundary-Layer Meteorol.*, **105,** 389–409

Zilitinkevich, S. S. and Chalikov, D. V. 1968 On the resistance and heat/moisture transfer laws in the interaction between the atmosphere and the underlying surface. *Izvestija AN SSSR, FAO*, **4,** No. 7, 765–772

Zilitinkevich, S. S. and Deardorff, J W. 1974 Similarity theory for the planetary boundary layer of time-dependent height. *J. Atmos. Sci.*, **31,** 1449–1452

Zilitinkevich, S. S. and Esau, I. N. 2002 On integral measures of the neutral, barotropic planetary boundary layers. *Boundary-Layer Meteorol.*, **104,** 371–379

2003 The effect of baroclinicity on the depth of neutral and stable planetary boundary layers. *Q. J. R. Meteorol. Soc.*, **129,** 3339–3356

Zilitinkevich, S. S. and Kreiman, K. D. 1991 Wind-induced drift of surface films. Chapter 4 in *Modelling air–lake interaction: Physical background.* Ed. S. S. Zilitinkevich. Springer-Verlag, Berlin, Germany

Zilitinkevich, S. S., Laikhtman, D. L. and Monin, A. S. 1967 Dynamics of the boundary layer in the atmosphere. *Izvestija, AN SSSR, FAO*, **3,** No. 3, 297–333

Zilitinkevich, S. S., Grachev, A. A. and Fairall, C. W. 2001 Scaling reasoning and field data on the sea-surface roughness lengths for scalars. *J. Atmos. Sci.*, **58,** 320–325